ARTICLE

doi:10.1038/nature23888

Rabies screen reveals GPe control of cocaine-triggered plasticity

Kevin T. Beier[1,2], Christina K. Kim[3], Paul Hoerbelt[1], Lin Wai Hung[1], Boris D. Heifets[1,4], Katherine E. DeLoach[2,7], Timothy J. Mosca[2,†], Sophie Neuner[1], Karl Deisseroth[5,6,7], Liqun Luo[2,7] & Robert C. Malenka[1]

Identification of neural circuit changes that contribute to behavioural plasticity has routinely been conducted on candidate circuits that were preselected on the basis of previous results. Here we present an unbiased method for identifying experience-triggered circuit-level changes in neuronal ensembles in mice. Using rabies virus monosynaptic tracing, we mapped cocaine-induced global changes in inputs onto neurons in the ventral tegmental area. Cocaine increased rabies-labelled inputs from the globus pallidus externus (GPe), a basal ganglia nucleus not previously known to participate in behavioural plasticity triggered by drugs of abuse. We demonstrated that cocaine increased GPe neuron activity, which accounted for the increase in GPe labelling. Inhibition of GPe activity revealed that it contributes to two forms of cocaine-triggered behavioural plasticity, at least in part by disinhibiting dopamine neurons in the ventral tegmental area. These results suggest that rabies-based unbiased screening of changes in input populations can identify previously unappreciated circuit elements that critically support behavioural adaptations.

Plasticity in neuronal circuits enables animals to adapt to an ever-changing environment. However, the loci and nature of experience-dependent changes in circuit function that drive adaptive and pathological behaviours remain largely unknown. Modern techniques such as optogenetics[1] and chemogenetics[2] permit the sequential screening of targeted elements in circuits with complex input and output patterns, but unbiased approaches are necessary to identify new components that play critical roles in the behavioural changes of interest. One such approach uses the expression of immediate early genes to identify the neuronal ensembles activated by a defined experience[3,4] but, as currently used, this approach does not reveal the connectivity of these ensembles. Brain imaging techniques such as functional MRI or positron-emission tomography also provide insights into unexpected experience-dependent macroscopic activity changes, but lack cellular resolution. Thus, there is a need for additional methods that facilitate unbiased identification of the circuit substrates of experience-dependent behavioural changes. Here, we present evidence that rabies virus-based monosynaptic tracing facilitates screening of circuit elements that contribute to behavioural changes by allowing whole-brain mapping of monosynaptic inputs[5,6] to defined starter neuronal populations and their input–output relationships[7–9].

To test the utility of a rabies virus-based approach for screening of behaviourally relevant experience-dependent circuit adaptations, we initially focused on the ventral tegmental area (VTA), a circuit node that is critical for a variety of experience-dependent behaviours[10–12]. The diverse array of inputs to and input–output relationships of dopamine and GABA (γ-aminobutyric acid) cells in the VTA have been extensively elucidated using rabies virus methods[5,7]. We used drugs of abuse as a robust trigger of experience-dependent plasticity, focusing on cocaine, which elicits long-lasting behavioural adaptations including locomotor sensitization (LMS) and conditioned place preference (CPP). Our unbiased input screen revealed an unexpected critical role for the GPe, which has been implicated in motor control[13], habit formation[14] and Parkinson's disease[15] but not studied in relation to addiction-related behaviours triggered by drugs of abuse. Our findings provide proof of principle for the utility of this approach while implicating the GPe in the establishment of drug-evoked behavioural plasticity.

Screen for cocaine-induced input changes

Cocaine administration induces modification of synapses on dopamine and GABA neurons in the VTA (VTA-DA and VTA-GABA neurons, respectively)[16] but the identities of cells providing those inputs are largely unknown. To test whether rabies virus monosynaptic tracing might reveal the identities of inputs altered by cocaine, we first used the rabies monosynaptic input tracing technique[17], where animals were given a single injection of cocaine (15 mg kg^{-1}) or saline one day before injection of the rabies virus, RV*dG* (Fig. 1a). Unbiased analysis of the labelled input cells from 22 brain regions comprising more than 90% of long-range inputs to VTA-DA neurons revealed that although the global maps were quantitatively similar, labelling proportionally increased or decreased in cocaine-treated animals in a small subset of regions, with inputs from the GPe displaying the largest proportional change (Fig. 1b).

To determine whether similar labelling changes occurred in response to different classes of abused substances, as occurs with synaptic adaptations onto VTA-DA neurons[16], we administered single doses of amphetamine, morphine, nicotine, or the psychoactive but non-addictive substance fluoxetine. The drugs of abuse increased labelling of GPe cells whereas fluoxetine did not (Fig. 1c, Extended Data Fig. 1a). As previous work using rabies virus revealed that VTA-DA and VTA-GABA neurons receive similar inputs[7], we next used the *GAD2-Cre* mouse driver line to test whether cocaine induced similar changes in labelling of cells making monosynaptic contacts onto midbrain GABA neurons in the VTA and the nearby substantia nigra pars reticulata (SNr) (Fig. 1d). Cocaine again elicited a proportional increase in labelling of GPe cells compared to saline injections (Fig. 1e).

[1]Nancy Pritzker Laboratory, Department of Psychiatry and Behavioral Sciences, Stanford University School of Medicine, Stanford, California 94305, USA. [2]Department of Biology, Stanford University, Stanford, California 94305, USA. [3]Neurosciences Program, Stanford University, Stanford, California 94305, USA. [4]Department of Anesthesiology, Perioperative and Pain Medicine, Stanford University School of Medicine, Stanford, California 94305, USA. [5]Department of Bioengineering, Stanford University, Stanford, California 94305, USA. [6]Department of Psychiatry and Behavioral Sciences, Stanford University School of Medicine, Stanford, California 94305, USA. [7]Howard Hughes Medical Institute, Stanford University, Stanford, California 94305, USA.
†Present address: Department of Neuroscience, Thomas Jefferson University, Philadelphia, Pennsylvania 19107, USA.

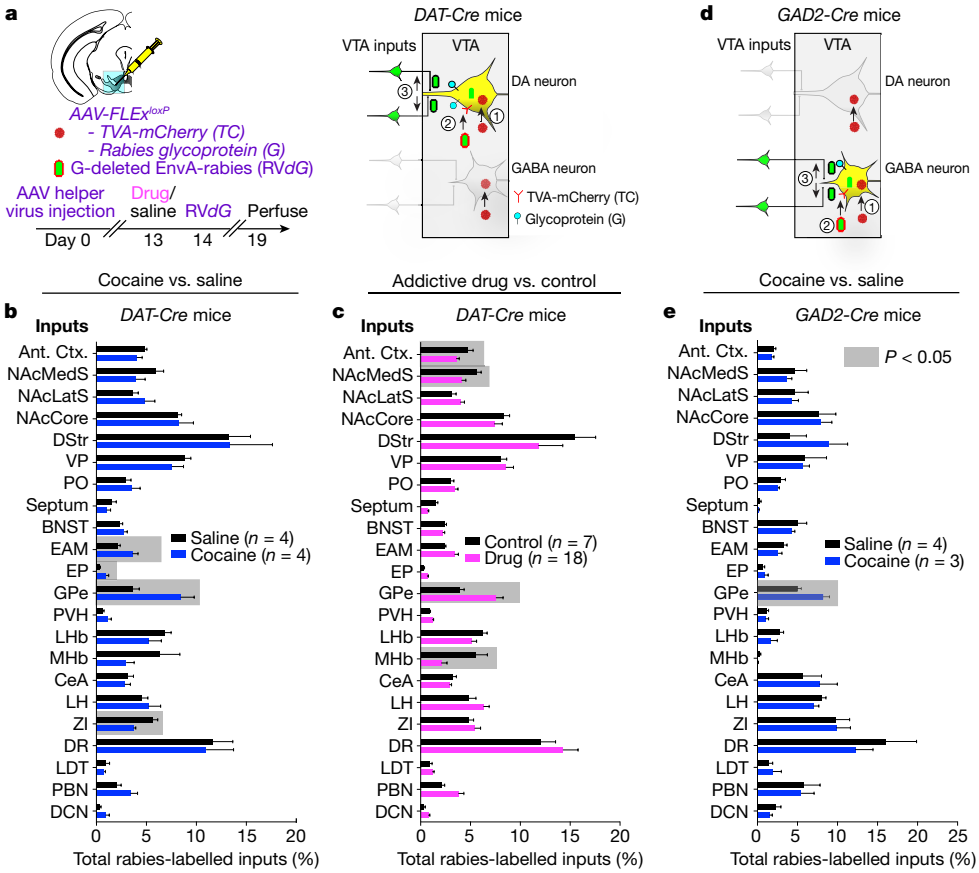

Figure 1 | Cocaine-induced changes to VTA neuron inputs. a, Strategy for labelling inputs to VTA-DA neurons. 1, 2, and 3 represent sequential steps in the experiment: AAV infection, rabies infection, and rabies spread. **b**, Fraction of total GFP$^+$ inputs from each site relative to total quantified inputs. Highlighted regions represent $P < 0.05$ ($P = 0.04$, 0.04, 0.02, 0.02 for EAM, EP, GPe, and ZI, respectively). **c**, Combined data for administration of drug of abuse ($n = 4$, 5, 5, 4 for cocaine, amphetamine, morphine, and nicotine, respectively) or control (saline, $n = 4$; fluoxetine, $n = 3$: $P = 0.005$, 0.007, 0.05, 0.05 for GPe, MHb, NAcMedS and anterior cortex, respectively). **d**, **e**, Strategy (**d**) and quantification (**e**) of labelling inputs to ventral midbrain GABA neurons (GPe, $P = 0.01$). For all figures, unless otherwise noted, statistical analyses used paired *t*-tests and error bars represent s.e.m. The schematics of the mouse brain in this figure were adapted from ref. 33. Ant. Ctx., anterior cortex; BNST, bed nucleus of the stria terminalis; CeA, central amygdala; DCN, deep cerebellar nuclei; DR, dorsal raphe; DStr, dorsal striatum; EAM, extended amygdala; EP, entopeduncular nucleus; LDT, laterodorsal tegmentum; LH, lateral hypothalamus; LHb, lateral habenula; MHb, medial habenula; NAcMedS/NAcLatS/NAcCore, nucleus accumbens medial shell/lateral shell/core; PBN, parabrachial nucleus; PO, preoptic nucleus; PVH, paraventricular hypothalamus; VP, ventral pallidum; ZI, zona incerta.

Cocaine enhances GPe–PV neuron activity

The four brain regions with the largest drug-induced change in labelling were the GPe, anterior cortex (Ant. Ctx.), medial habenula (MHb), and nucleus accumbens medial shell (NAcMedS) (Fig. 1c, Extended Data Fig. 1a). While the latter three have been previously implicated in the behavioural adaptations caused by drugs of abuse[11], the potential role of the GPe has not been investigated, to our knowledge. To investigate what the increase in rabies virus labelling of GPe inputs onto VTA-DA and VTA-GABA cells tells us about the effects of cocaine, we used parvalbumin (*Pvalb*)-*Cre* or *Pvalb-Flp* mouse driver lines to specifically target parvalbumin neurons in the GPe (GPe-PV cells) (as the majority of rabies-labelled GPe cells making synapses onto VTA-DA neurons co-stained with parvalbumin (305 of 367; Extended Data Fig. 1b)). Visualization of axons of GPe-PV neurons expressing a membrane-tagged GFP demonstrated that these cells send major projections to a range of brain regions, including the forebrain and thalamus (Extended Data Fig. 2a, b). Consistent with previous work[18], the main GPe projection to the midbrain was to the SNr, which contains mostly GABA neurons[19], while dopamine neuron-containing nuclei such as the substantia nigra pars compacta (SNc) or VTA received fewer inputs (Extended Data Fig. 2c, d).

To determine whether the cocaine-induced increase in rabies virus labelling of GPe cells reflected an increase in the number of synaptic contacts, we injected the adeno-associated virus (AAV) *AAV-FLEx^{loxP}-mGFP-2A-synaptophysin-mRuby,* which labels putative presynaptic sites (Fig. 2a), into the GPe of *Pvalb-Cre* mice and imaged them after a cocaine or saline injection about 1 month later (Fig. 2b). The density and volume of labelled puncta in the SNr were indistinguishable in saline versus cocaine-treated animals (Fig. 2c, d), suggesting that there was no change in synapse number. Next, we assessed potential changes in synapse strength, as single doses of drugs of abuse can enhance the synaptic strength of both excitatory and inhibitory inputs into the ventral midbrain[16]. We injected a Flp-dependent AAV expressing channelrhodopsin (*AAV-FLEx^{FRT}-ChR2*) into the GPe of *Pvalb-Flp* mice and conducted whole-cell recordings from SNr neurons in acute slices about 1 month later. Calcium in the extracellular recording solution was replaced by strontium to enable measurement of quantal events[20] (Fig. 2e, f). No change in the amplitude or frequency of quantal events was observed in slices prepared from cocaine- versus saline-treated mice (Fig. 2g, h), suggesting that cocaine did not elicit a change in the strength of the inhibitory synapses made by GPe-PV neurons onto SNr neurons.

Finally, we assessed whether the spontaneous activity of GPe-PV neurons *in vivo* was altered by cocaine by expressing the fluorescent Ca^{2+} indicator GCaMP6f in GPe-PV neurons and collecting population Ca^{2+}-dependent signals using fibre photometry (Fig. 2i). Although

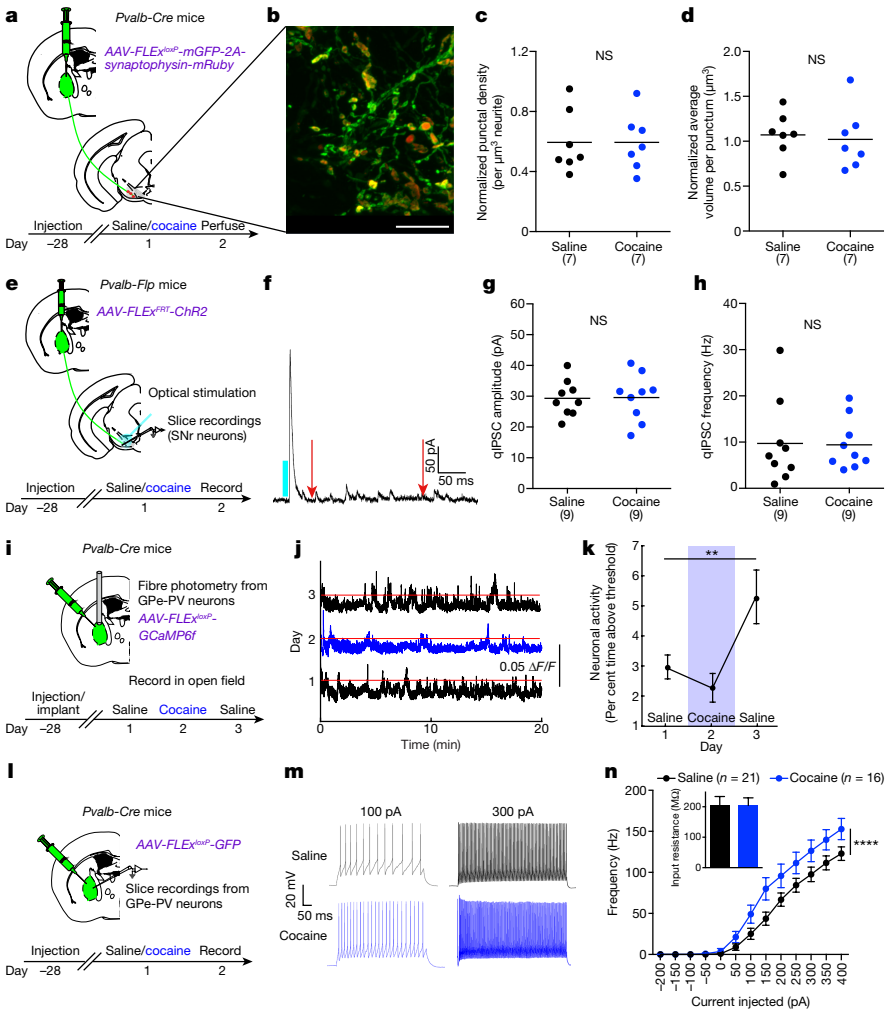

Figure 2 | Cocaine triggers increase in GPe-PV neuron activity and excitability. **a**–**d**, Measurement of synapse number. **a**, *AAV-FLEx^{loxP}-mGFP-2A-synaptophysin-mRuby* was injected into the GPe of *Pvalb-Cre* mice to quantify mRuby$^+$ puncta in the SNr. **b**, mGFP$^+$ neurites (green) and mRuby$^+$ puncta (red) from GPe-PV neurons in the SNr (scale bar, 10 μm). **c**, **d**, No change in density (**c**; $P = 0.99$) or volume (**d**; $P = 0.76$) of mRuby$^+$ puncta was observed. **e**–**h**, Measurement of synapse strength. **e**, *AAV-FLEx^{FRT}-ChR2* was injected into the GPe of *Pvalb-Flp* mice, and recordings conducted from SNr-GABA neurons in slices from cocaine- or saline-treated animals. **f**, Trace from SNr neuron highlighting the time window for analysis. Red arrows indicate the segment of the trace that was analysed for quantal events. **g**, **h**, No change in quantal IPSC amplitude (**g**; $P = 0.94$) or frequency (**h**; $P = 0.94$) was observed. **i**–**k**, Measurement of input activity. **i**, *AAV-FLEx^{loxP}-GCaMP6f* was injected into the GPe of *Pvalb-Cre* mice to measure GPe-PV neuron activity using fibre photometry. **j**, Traces showing $\Delta F/F$ following the first saline, cocaine, and second saline injections. Red line shows activity threshold of six times the median absolute deviation. **k**, Per cent time for which activity surpassed threshold (one-way ANOVA, $P = 0.018$; *post hoc* tests day 1 vs. 2, $P = 0.17$; day 1 vs. 3, $P = 0.0049$). **l**–**n**, Measurement of excitability. **l**, *AAV-FLEx^{loxP}-GFP* was injected into the GPe of *Pvalb-Cre* mice, and recordings made from GFP$^+$ cells. **m**, Traces from depolarizing current injections. **n**, Frequency of action potentials over range of current steps ($P < 0.0001$ for saline vs. cocaine, two-way ANOVA). For all figures: NS, not significant ($P > 0.05$), *$P \leq 0.05$, **$P \leq 0.01$, ***$P \leq 0.001$, ****$P \leq 0.0001$. Dot plots include horizontal line representing mean. The schematics of the mouse brain in this figure were adapted from ref. 33.

cocaine administration had no significant acute effect, population activity had increased twofold by the following day (Fig. 2j, k). To assess whether this increase might reflect changes in intrinsic excitability, we injected *AAV-FLEx^{loxP}-GFP* into the GPe of *Pvalb-Cre* mice and made targeted whole-cell current clamp recordings from acute GPe slices prepared one day after the mice received saline or cocaine injections (Fig. 2l). GPe-PV neurons from cocaine-treated mice were more excitable, in that more action potentials were generated by depolarizing current injection steps (Fig. 2m, n) with no change in the input resistances of the cells (Fig. 2n). These results demonstrate that a single exposure to cocaine triggers increases in the spontaneous activity and excitability of GPe-PV neurons.

Input activity modulates rabies labelling

To investigate whether the cocaine-induced changes in rabies virus labelling of GPe-PV input neurons result from the observed changes in their activity, we expressed transgenes in GPe-PV neurons that permit manipulation of their activity levels while simultaneously performing rabies virus transsynaptic labelling. Chronic activity manipulations bidirectionally influenced the extent of GPe neuronal labelling: chronic inhibition of GPe-PV neuron activity with the inhibitory DREADD hM4Di[2] or $K_{ir}2.1$[21] decreased rabies virus labelling of GPe neurons compared to control and yellow fluorescent protein (YFP)-expressing mice, whereas excitation using hM3Dq[2], on average, increased labelling (Fig. 3d). As a control for these manipulations, we examined labelling in the NAcMedS and found no effect due to expressing any of these transgenes in GPe-PV neurons (Fig. 3e).

To determine whether the effects of chronic activity changes on rabies virus transsynaptic labelling generalized to other brain regions, we performed the same genetic manipulations on D1 receptor-expressing medium spiny neurons (MSNs) in the NAcMedS, the labelling of which was decreased by drugs of abuse (Fig. 1c, Extended Data Fig. 1a, c). Parallel to the effects of manipulating GPe-PV neurons, chronic NAcMedS inhibition using hM4Di or $K_{ir}2.1$ reduced labelled inputs into the NAcMedS, whereas activation with hM3Dq enhanced NAcMedS labelling (Fig. 3h). Unexpectedly, although NAcMedS inhibition did not alter labelling of GPe neurons, NAcMedS activation increased labelled GPe inputs (Fig. 3g), suggesting that activation of D1 MSNs in the NAcMedS indirectly increases GPe activity. Together, these experiments provide evidence that rabies-mediated transsynaptic labelling from starter neurons is influenced by the level of activity in input cell populations. Furthermore, they support the hypothesis that cocaine and other drugs of abuse chronically increase the level of GPe-PV neuron activity and that this accounts for the observed increase in GPe neuron labelling by the rabies virus.

Behavioural changes require GPe activity

To determine whether the cocaine-elicited changes in GPe-PV neuron activity revealed by rabies virus tracing are functionally relevant and necessary for cocaine-induced behavioural adaptations, we tested whether inhibition of GPe-PV neurons influenced two forms of cocaine-induced behavioural plasticity, LMS and CPP. Inhibition of activity in GPe-PV neurons using expression of any one of three transgenes—encoding hM4Di, $K_{ir}2.1$ or the tetanus toxin light chain (TeTxLc), which inhibits presynaptic vesicle release[22]—prevented cocaine-induced LMS (Fig. 4a–c), while having no effect on basal locomotion and only a modest effect on cocaine-induced locomotion upon initial administration (Extended Data Fig. 3). Furthermore,

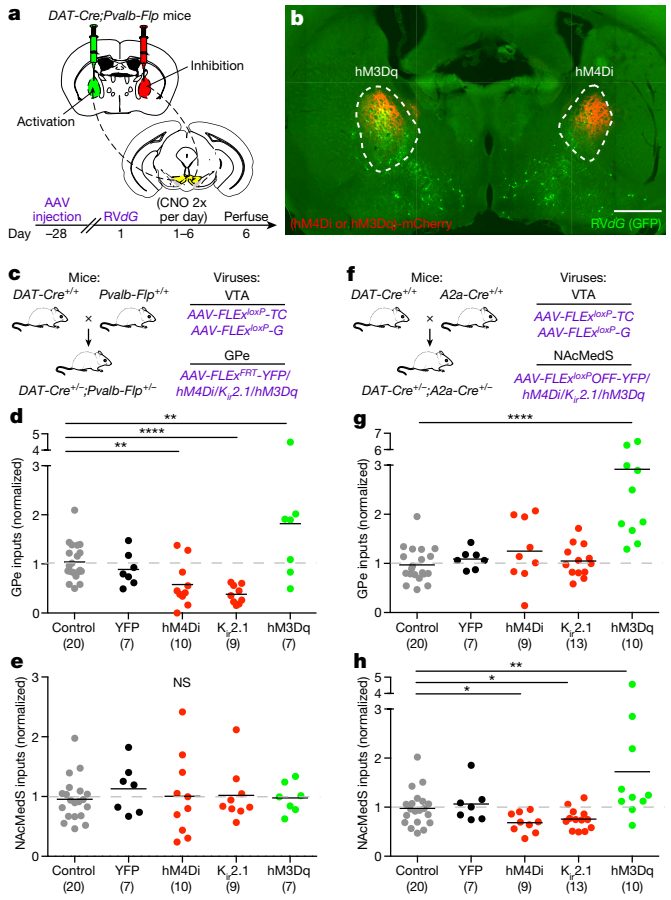

Figure 3 | Bidirectional modulation of rabies labelling by activity manipulations. a, A mixture of *AAV-FLEx^{loxP}-TC* and *AAV-FLEx^{loxP}-G* was injected into the VTA while an AAV expressing a Flp-dependent YFP, hM4Di, $K_{ir}2.1$ or hM3Dq was injected into the GPe. **b**, Rabies labelling in GPe (scale bar, 1 mm). **c**–**e**, GPe manipulation. **c**, Experimental strategy. **d**, Quantification of labelled inputs in GPe. *y*-axis shows labelled GPe inputs/(NAcLatS + NAcCore inputs). Combined controls (uninjected and YFP) were assigned a value of 1. GPe inhibition reduced (hM4Di, $P = 0.004$; $K_{ir}2.1$, $P < 0.0001$) and activation increased (hM3Dq, $P = 0.016$) labelled inputs. **e**, Quantification of labelled inputs in NAcMedS (hM4Di, $P = 0.98$; $K_{ir}2.1$, $P = 0.90$; hM3Dq, $P = 0.88$). **f**–**h**, NAcMedS manipulation. **f**, Experimental strategy. **g**, NAcMedS-D1 inhibition had no effect on labelling of GPe inputs (hM4Di, $P = 0.13$; $K_{ir}2.1$, $P = 0.65$) while activation increased labelling (hM3Dq, $P < 0.001$). **h**, NAcMedS-D1 inhibition decreased (hM4Di, $P = 0.02$; $K_{ir}2.1$, $P = 0.03$) while activation increased (hM3Dq, $P = 0.007$) labelling of NAcMedS inputs. The schematics of the mouse brain in this figure were adapted from ref. 33.

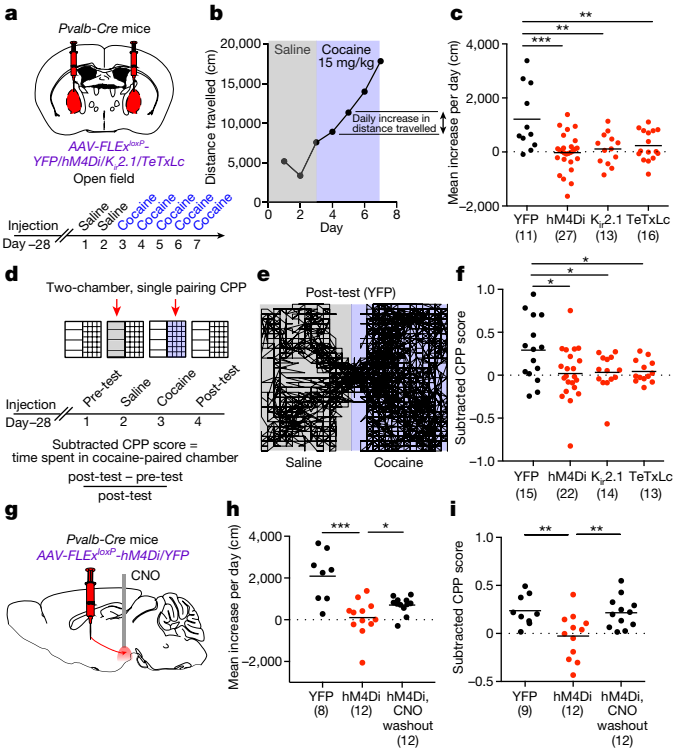

Figure 4 | GPe-PV neuron activity is required for cocaine-induced LMS and CPP. a, Cre-dependent AAVs were injected into the GPe of *Pvalb-Cre* mice. **b**, **c**, Locomotor sensitization. **b**, Plot of locomotor activity for a single mouse. **c**, GPe-PV neuron inhibition blocked cocaine-induced LMS (hM4Di, $P = 0.0002$; $K_{ir}2.1$, $P = 0.007$; TeTxLc, $P = 0.008$). **d**–**f**, Conditioned place preference. **d**, Procedure to test CPP during GPe-PV neuron inhibition. **e**, Trace from YFP mouse during post-test. **f**, GPe-PV neuron inhibition prevented CPP (hM4Di, $P = 0.019$; $K_{ir}2.1$, $P = 0.030$; TeTxLc, $P = 0.029$). **g**–**i**, Inhibition of GPe-PV projections to midbrain. **g**, Slow-release CNO microspheres were injected into ventral midbrain in animals expressing hM4Di or YFP in GPe-PV neurons. **h**, **i**, Both LMS (**h**; $P = 0.0005$) and CPP (**i**; $P = 0.0094$) were blocked in hM4Di-expressing animals. When tested again after CNO washout, the same mice developed LMS (**h**; $P = 0.047$) and CPP (**i**; $P = 0.0078$). The schematics of the mouse brain in this figure were adapted from ref. 33.

there was a positive correlation between the number of rabies-labelled GPe inputs and the magnitude of LMS in a two-day injection protocol for cocaine as well as other addictive drugs (Extended Data Fig. 4). Similar results were obtained for cocaine-elicited CPP: using a four-day protocol (Fig. 4d), inhibition of GPe-PV activity through expression of hM4Di, $K_{ir}2.1$ or TeTxLc prevented CPP (Fig. 4e, f). Inhibition of GPe-PV neurons with hM4Di also prevented morphine-induced LMS and CPP (Extended Data Fig. 5), implying that the role of these neurons may generalize to other abused substances.

A limitation of these experiments is that GPe-PV neurons project to several brain regions (Extended Data Fig. 2) and thus the transgene-mediated inhibition of these neurons was not target-specific. To limit the expression of an inhibitory transgene specifically to those GPe-PV neurons that project to the midbrain, we injected the retrogradely transported *CAV-FLEx^{loxP}-Flp* into the midbrain of *Pvalb-Cre* mice and the Flp-dependent *AAV-FLEx^{FRT}-K$_{ir}$2.1* into the GPe, enabling $K_{ir}2.1$ expression to be restricted to Cre-expressing GPe-PV neurons projecting to the midbrain (Extended Data Fig. 6a). This manipulation prevented both cocaine-elicited LMS and CPP (Extended Data Fig. 6b, c). However, subsequent axon tracing experiments revealed that the GPe-PV neurons projecting to the midbrain collateralize extensively (Extended Data Fig. 7), limiting the interpretation of this experiment. To inhibit the GPe-PV neuron projections within the midbrain specifically, we expressed hM4Di in GPe-PV neurons and infused slow-release clozapine *N*-oxide (CNO) microspheres[23] into the midbrain (Fig. 4g). This local inhibition was sufficient to block cocaine-induced LMS (Fig. 4h) and CPP (Fig. 4i). After waiting a week to allow depletion of CNO, the same mice were re-tested using the same protocols, and expressed significant LMS and CPP (Fig. 4h, i). These results demonstrate that activity in the projection of GPe-PV neurons to the midbrain is necessary for two forms of cocaine-induced behavioural plasticity.

GPe–PV neurons disinhibit VTA–DA neurons

Does the cocaine-induced increase in activity in inhibitory GPe-PV neurons influence dopamine neuron activity, which is required for induction of LMS and CPP (Extended Data Fig. 8)? Given that the major projection from GPe-PV neurons to the midbrain is into the SNr (Extended Data Fig. 2), a simple hypothesis is that GPe-PV neurons strongly inhibit SNr neurons that tonically inhibit dopamine neurons. Thus, activation of GPe-PV neurons would increase dopamine neuron

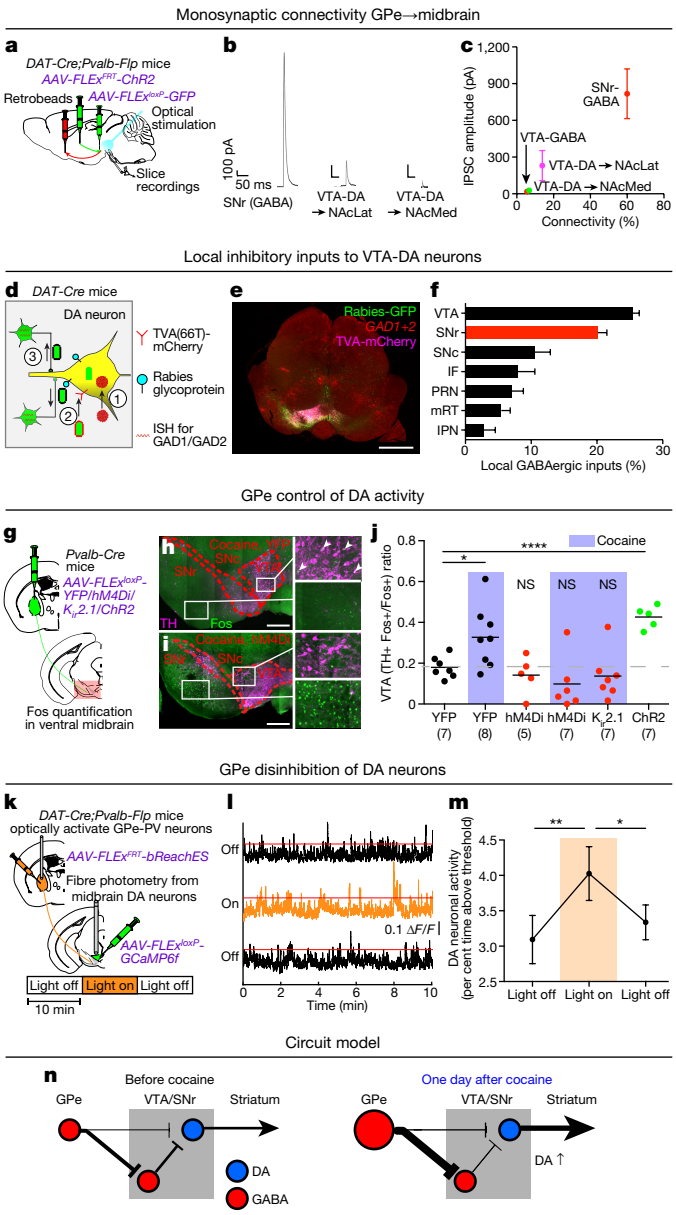

Figure 5 | GPe-PV neurons disinhibit VTA-DA neurons. **a**–**c**, Monosynaptic connectivity between GPe and midbrain. **a**, *AAV-FLEx^{FRT}-ChR2* was injected into the GPe, *AAV-FLEx^{loxP}-GFP* injected into the VTA, and retrobeads injected into the NAcLatS or NAcMedS of *DAT-Cre;Pvalb-Flp* or *GAD2-Cre;Pvalb-Flp* mice. Whole-cell recordings were made from identified midbrain neurons in acute slices. **b**, Example light-evoked IPSCs. **c**, Quantification of per cent connectivity and IPSC amplitude for each cell type. **d**–**f**, Local inhibitory inputs to VTA-DA neurons. **d**, *AAV-FLEx^{loxP}-TC66T* and *AAV-FLEx^{loxP}-G* were injected into the VTA of *DAT-Cre* mice, followed two weeks later by RV*dG*. **e**, Sample labelling of midbrain section (scale bar, 1 mm). **f**, Quantification of labelled local inhibitory inputs. **g**–**j**, GPe control of dopamine neuron activity. **g**, Cre-dependent AAVs expressing YFP, hM4Di, $K_{ir}2.1$ or ChR2 were injected into the GPe of *Pvalb-Cre* mice followed by quantification of Fos labelling after manipulations. **h**, **i**, Sections of ventral midbrain showing Fos labelling (green) and tyrosine hydroxylase (TH) labelling (magenta) in animals receiving cocaine injections and expressing YFP (**h**) or hM4Di (**i**) in GPe. Arrows indicate Fos$^+$ neurons co-expressing tyrosine hydroxylase (scale bar, 200 μm). **j**, Quantification of activated dopamine neurons (Fos$^+$ TH$^+$) relative to all activated ventral midbrain neurons (Fos$^+$) (cocaine–YFP, $P = 0.029$; ChR2, $P < 0.0001$). **k**–**m**, GPe disinhibition of dopamine neurons. **k**, Flp-dependent bReachES was injected into the GPe and a Cre-dependent GCaMP6f was injected into the VTA of *DAT-Cre;Pvalb-Flp* mice. **l**, Fibre photometry traces during consecutive 10-min epochs. **m**, VTA-DA neurons were more active during light-on than light-off (one-way ANOVA, $P = 0.014$; *post hoc* tests 0–10 vs. 10–20 min, $P = 0.008$; 10–20 vs. 20–30 min, $P = 0.039$). **n**, Proposed circuit diagram before and after cocaine. Sizes of cell bodies and arrows represent activity strength. The schematics of the mouse brain in this figure were adapted from ref. 33.

activity via disinhibition, despite some direct synaptic inhibition of dopamine neurons. We tested this hypothesis in several ways. First, to examine the functional strength of GPe-PV neuron connections to midbrain dopamine and GABA neurons, we injected *AAV-FLEx^{FRT}-ChR2* into the GPe of either *DAT-Cre;Pvalb-Flp* (*DAT* is also known as *Slc6a3*) or *GAD2-Cre;Pvalb-Flp* double transgenic mice, *AAV-FLEx^{loxP}-GFP* into the VTA to label dopamine or GABA neurons (Fig. 5a), and retrobeads into either the NAcMedS or nucleus accumbens lateral shell (NAcLatS) to demarcate one of two VTA-DA subpopulations whose inputs are modified by cocaine[24]. We then measured monosynaptic inhibitory postsynaptic currents (IPSCs) by whole-cell recordings in acute slices. Optical stimulation of GPe-PV neuron axons evoked large IPSCs in the majority (63%, $n = 24$) of SNr-GABA neurons (Fig. 5b, c). In the same sets of slices using the same optical stimulation, the connectivity onto VTA neurons was much smaller (5–14%), as was the size of the IPSCs in cells in which they could be detected (Fig. 5b, c, Extended Data Fig. 9). These results demonstrate that functionally, GPe-PV neurons exhibit much stronger inhibitory connections onto SNr-GABA neurons than onto VTA-DA or VTA-GABA neurons, and thus the GPe-PV synapses in the VTA appear to be of limited functional importance.

Second, we tested whether manipulating activity in SNr-GABA neurons could alter the development of LMS and CPP. Activation of SNr-GABA neurons with hM3Dq prevented the development of LMS and CPP (Extended Data Fig. 10a–c), whereas concurrently inhibiting SNr-GABA neurons with hM4Di during chronic GPe-PV neuron inhibition rescued cocaine-mediated behavioural plasticity (Extended Data Fig. 10d–f). These results suggest that GPe-PV neuron inhibition prevents LMS and CPP by enhancing the activity of SNr-GABA neurons.

Third, we examined whether SNr-GABA neurons provide direct inhibition to dopamine neurons using a modified rabies virus input tracing strategy[25] to label local inputs onto dopamine neurons and combining this with *in situ* hybridization for *Gad1* and *Gad2* mRNA (Fig. 5d, e). Quantitatively, SNr-GABA neurons were the second-largest source of inhibitory inputs to dopamine neurons (Fig. 5f).

Fourth, we tested whether changes in GPe-PV neuron activity influenced integrated VTA-DA neuron activity using Fos labelling. In YFP-expressing mice, acute cocaine administration caused a clear increase in Fos$^+$ dopamine neurons compared to saline-injected mice 90 min after injection (Fig. 5j). Inhibition of GPe-PV neurons with hM4Di had no effect in saline-treated animals but completely prevented the increase in cocaine-treated mice, as did expression of $K_{ir}2.1$ (Fig. 5j). Conversely, activation of GPe-PV neurons by ChR2 increased Fos expression in dopamine neurons to a degree similar to that elicited by cocaine (Fig. 5j).

Finally, to test the effect of activating GPe-PV neurons on VTA-DA neuron activity directly *in vivo*, we injected a Flp-dependent red-shifted opsin (bReachES)[26] into the GPe and a Cre-dependent GCaMP6f into the VTA of *DAT-Cre;Pvalb-Flp* double transgenic mice, and recorded population activity from midbrain dopamine neurons with fibre photometry while optically activating GPe-PV neurons (Fig. 5k). Stimulation of GPe-PV neurons caused a small but significant increase in GCaMP6f fluorescence in VTA-DA neurons (Fig. 5l, m). Together, these results indicate that GPe-PV neurons control VTA-DA neuron activity through disynaptic disinhibition via SNr-GABA neurons (Fig. 5n).

Concluding remarks

The association of specific experience-dependent circuit changes with corresponding behavioural adaptations has been hampered by a lack of suitable methodology. While most investigations of circuit function rely on a candidate approach that takes advantage of cell-type specific manipulations, such studies are limited by the requirement for *a priori* assumptions regarding the roles of targeted populations. Given the complexity of circuit mechanisms that mediate animal behaviours, unbiased approaches offer advantages for identifying the array of specific neuroplastic changes that drive behavioural changes. Here, we demonstrate that neural activity influences the extent of labelling by the rabies monosynaptic input tracing method. This property enabled us to identify circuit elements that were modified by experience in a behaviourally relevant manner. Specifically, the activity-dependence of rabies labelling enabled us to identify an underappreciated circuit node, the GPe, as a key player in cocaine-induced behavioural adaptations. As a core component of the dorsal striatal indirect pathway implicated in motor control[13] and associated disorders[15,27], the GPe had not previously (to our knowledge) been directly linked to addictive behaviours. Using a number of different assays, we demonstrated that the effect of enhanced GPe input to the midbrain is to increase VTA-DA neuron activity via a mechanism of disinhibition (Fig. 5n). Our findings provide a novel circuit mechanism for influencing VTA-DA neuron activity, and confirm that this mechanism has a critical role in drug-induced behavioural adaptations[11,28] (Extended Data Fig. 8). Given that the rabies virus transsynaptic technique has been used successfully to map inputs onto cell populations in many brain areas[5–9,29–32], we anticipate that this method will be generalizable and complementary to other circuit analysis methods[1,2] for elucidating how activity changes in connected ensembles orchestrate features of complex behaviours.

Online Content Methods, along with any additional Extended Data display items and Source Data, are available in the online version of the paper; references unique to these sections appear only in the online paper.

Received 24 March; accepted 31 July 2017.
Published online 13 September 2017.

1. Boyden, E. S., Zhang, F., Bamberg, E., Nagel, G. & Deisseroth, K. Millisecond-timescale, genetically targeted optical control of neural activity. *Nat. Neurosci.* **8,** 1263–1268 (2005).
2. Armbruster, B. N., Li, X., Pausch, M. H., Herlitze, S. & Roth, B. L. Evolving the lock to fit the key to create a family of G protein-coupled receptors potently activated by an inert ligand. *Proc. Natl Acad. Sci. USA* **104,** 5163–5168 (2007).
3. Lin, D. *et al.* Functional identification of an aggression locus in the mouse hypothalamus. *Nature* **470,** 221–226 (2011).
4. Ye, L. *et al.* Wiring and molecular features of prefrontal ensembles representing distinct experiences. *Cell* **165,** 1776–1788 (2016).
5. Watabe-Uchida, M., Zhu, L., Ogawa, S. K., Vamanrao, A. & Uchida, N. Whole-brain mapping of direct inputs to midbrain dopamine neurons. *Neuron* **74,** 858–873 (2012).
6. Weissbourd, B. *et al.* Presynaptic partners of dorsal raphe serotonergic and GABAergic neurons. *Neuron* **83,** 645–662 (2014).
7. Beier, K. T. *et al.* Circuit architecture of VTA dopamine neurons revealed by systematic input-output mapping. *Cell* **162,** 622–634 (2015).
8. Schwarz, L. A. *et al.* Viral-genetic tracing of the input-output organization of a central noradrenaline circuit. *Nature* **524,** 88–92 (2015).
9. Lerner, T. N. *et al.* Intact-brain analyses reveal distinct information carried by SNc dopamine subcircuits. *Cell* **162,** 635–647 (2015).
10. Lammel, S. *et al.* Input-specific control of reward and aversion in the ventral tegmental area. *Nature* **491,** 212–217 (2012).
11. Kalivas, P. W. & Volkow, N. D. The neural basis of addiction: a pathology of motivation and choice. *Am. J. Psychiatry* **162,** 1403–1413 (2005).
12. Nestler, E. J. & Carlezon, W. A. Jr. The mesolimbic dopamine reward circuit in depression. *Biol. Psychiatry* **59,** 1151–1159 (2006).
13. Albin, R. L., Young, A. B. & Penney, J. B. The functional anatomy of basal ganglia disorders. *Trends Neurosci.* **12,** 366–375 (1989).
14. Yin, H. H. & Knowlton, B. J. The role of the basal ganglia in habit formation. *Nat. Rev. Neurosci.* **7,** 464–476 (2006).
15. Hammond, C., Bergman, H. & Brown, P. Pathological synchronization in Parkinson's disease: networks, models and treatments. *Trends Neurosci.* **30,** 357–364 (2007).
16. Lüscher, C. & Malenka, R. C. Drug-evoked synaptic plasticity in addiction: from molecular changes to circuit remodeling. *Neuron* **69,** 650–663 (2011).
17. Wickersham, I. R. *et al.* Monosynaptic restriction of transsynaptic tracing from single, genetically targeted neurons. *Neuron* **53,** 639–647 (2007).
18. Smith, Y. & Bolam, J. P. The output neurones and the dopaminergic neurones of the substantia nigra receive a GABA-containing input from the globus pallidus in the rat. *J. Comp. Neurol.* **296,** 47–64 (1990).
19. Zhou, F.-M. & Lee, C. R. Intrinsic and integrative properties of substantia nigra pars reticulata neurons. *Neuroscience* **198,** 69–94 (2011).
20. Oliet, S. H. R., Malenka, R. C. & Nicoll, R. A. Bidirectional control of quantal size by synaptic activity in the hippocampus. *Science* **271,** 1294–1297 (1996).
21. Raab-Graham, K. F., Radeke, C. M. & Vandenberg, C. A. Molecular cloning and expression of a human heart inward rectifier potassium channel. *Neuroreport* **5,** 2501–2505 (1994).
22. Schiavo, G. *et al.* Tetanus and botulinum-B neurotoxins block neurotransmitter release by proteolytic cleavage of synaptobrevin. *Nature* **359,** 832–835 (1992).
23. Stachniak, T. J., Ghosh, A. & Sternson, S. M. Chemogenetic synaptic silencing of neural circuits localizes a hypothalamus→midbrain pathway for feeding behavior. *Neuron* **82,** 797–808 (2014).
24. Lammel, S., Ion, D. I., Roeper, J. & Malenka, R. C. Projection-specific modulation of dopamine neuron synapses by aversive and rewarding stimuli. *Neuron* **70,** 855–862 (2011).
25. Miyamichi, K. *et al.* Dissecting local circuits: parvalbumin interneurons underlie broad feedback control of olfactory bulb output. *Neuron* **80,** 1232–1245 (2013).
26. Rajasethupathy, P. *et al.* Projections from neocortex mediate top-down control of memory retrieval. *Nature* **526,** 653–659 (2015).
27. Gittis, A. H. *et al.* New roles for the external globus pallidus in basal ganglia circuits and behavior. *J. Neurosci.* **34,** 15178–15183 (2014).
28. Pierce, R. C. & Kumaresan, V. The mesolimbic dopamine system: the final common pathway for the reinforcing effect of drugs of abuse? *Neurosci. Biobehav. Rev.* **30,** 215–238 (2006).
29. Stepien, A. E., Tripodi, M. & Arber, S. Monosynaptic rabies virus reveals premotor network organization and synaptic specificity of cholinergic partition cells. *Neuron* **68,** 456–472 (2010).
30. Miyamichi, K. *et al.* Cortical representations of olfactory input by trans-synaptic tracing. *Nature* **472,** 191–196 (2011).
31. Yonehara, K. *et al.* Spatially asymmetric reorganization of inhibition establishes a motion-sensitive circuit. *Nature* **469,** 407–410 (2011).
32. Wall, N. R., De La Parra, M., Callaway, E. M. & Kreitzer, A. C. Differential innervation of direct- and indirect-pathway striatal projection neurons. *Neuron* **79,** 347–360 (2013).
33. Franklin, K. B. J. & Paxinos, G. *The Mouse Brain in Stereotaxic Coordinates* 4th edn (Academic, 2012).

Supplementary Information is available in the online version of the paper.

Acknowledgements This study was supported by grants from the Howard Hughes Medical Institute (Hughes Collaborative Innovation Award), National Institutes of Health (R01-NS50835, PO1 DA008227, TR01-MH099647, F32-DA038913, K99-DC013059 and K99-DA041445), and the Stanford Neurosciences Institute.

Author Contributions K.T.B. performed the majority of experiments and data analysis; C.K.K. assisted with fibre photometry experiments and data analysis with support from K.D; P.H. assisted with electrophysiological recordings and data analysis; L.W.H. performed surgeries for ChR2 stimulation and Fos counting; B.D.H. assisted with terminal inhibition experiments; T.J.M. assisted with assay design for puncta quantification; K.E.D. and S.N. provided technical support; K.T.B., L.L. and R.C.M. designed the experiments, interpreted the results and wrote the paper, which was edited by all authors.

Author Information Reprints and permissions information is available at www.nature.com/reprints. The authors declare competing financial interests: details are available in the online version of the paper. Readers are welcome to comment on the online version of the paper. Publisher's note: Springer Nature remains neutral with regard to jurisdictional claims in published maps and institutional affiliations. Correspondence and requests for materials should be addressed to L.L. (lluo@stanford.edu) or R.C.M. (malenka@stanford.edu).

Reviewer Information *Nature* thanks P. Kenny, M. Wolf and the other anonymous reviewer(s) for their contribution to the peer review of this work.

METHODS

No statistical methods were used to predetermine sample size. Experiments described in Figs 1, 2a–h, l–n, 3, and 5g–j and Extended Data Figs 1a, 4, 5, 6, 8 and 10 were randomized and investigators were blinded to allocation and outcome assessments; all other experiments were not randomized and investigators were not blinded.

Mice and viral procedures. Generation and characterization of the *DAT-Cre*[34], *GAD2-Cre*[35], *Pvalb-Cre*[36], *Pvalb-Flp*[37], *A2a-Cre*[38], and *D1-tdtomato*[39] mouse lines have been described previously. Mice were housed on a 12-h light–dark cycle with food and water *ad libitum*. Males and females from a mixed CD1 and C57/BL6 background were used for all experiments in approximately equal proportions. All surgeries were done under isoflurane anaesthesia. All procedures complied with the animal care standards set forth by the National Institute of Health and were approved by Stanford University's Administrative Panel on Laboratory Animal Care and Administrative Panel of Biosafety.

pAAV-CAG-FLEx^{loxP}-G, *pAAV-CAG-FLEx^{loxP}-TC*, *pAAV-CAG-FLEx^{loxP}-TC66T*, *pAAV-CAG-FLEx^{FRT}-G*, *pAAV-CAG-FLEx^{FRT}-TC*, *pAAV-hsyn1-FLEx^{loxP}-mGFP-2A-synaptophysin-mRuby*, and *pCAV-FLEx^{loxP}-Flp* were constructed as reported previously[8]. For construction of viruses containing YFP, *K$_{ir}$2.1-2A-GFP*, *hM4Di-mCherry*, and *hM3Dq-mCherry*, *pAAV-hsyn1-FLEx^{loxP}-mGFP-2A-synaptophysin-mRuby*[9] or *pAAV-hsyn1-FLEx^{FRT}-mGFP-2A-synaptophysin-mRuby*[7] were used as templates. All inserts were cloned into the AscI and SalI sites between the *loxP* or *FRT* sites. *hM3Dq-mCherry* or *hM4Di-mCherry* were PCR-amplified from *pAAV-hsyn1-DIO-hM3Dq-mCherry* or *pAAV-hsyn1-DIO-hM4Di-mCherry*, respectively[40], and *K$_{ir}$2.1-2A-GFP* was modified from Xue *et al.*[41]. *AAV-CMV-FLEx^{loxP}-GFP-2A-TeTxLc*, *AAV-hsyn1-FLEx^{loxP}-ChR2(H134R)-eYFP*, *AAV-hsyn1-FLEx^{loxP}-eYFP*, and *AAV-hsyn1-FLEx^{FRT}-eYFP* were purchased from the Stanford Gene and Viral Vector Core.

Transsynaptic tracing. Transsynaptic tracing studies were carried out as previously described[7], with minor modifications. For rabies tracing, 100 nl of a 1:1 volume mixture of *AAV-CAG-FLEx^{loxP}-TC* and *AAV-CAG-FLEx^{loxP}-G* was injected into the VTA of 4–6-week-old mice. Thirteen days later, a single dose of cocaine (15 mg/kg), amphetamine (10 mg/kg), nicotine (0.5 mg/kg), morphine (10 mg/kg), fluoxetine (10 mg/kg) or saline was injected intraperitoneally (IP), and the mouse was placed in a new cage for thirty minutes before being returned to its home cage. On the following day, RV*dG* was injected into the VTA. After recovery, mice were housed in a BSL2 facility for 5 days to allow rabies spread and GFP expression. *P* values presented in Fig. 1 were not corrected for multiple comparisons.

For identification of local GABAergic inputs to VTA-DA neurons, 100 nl of a 1:1 volume mixture of *AAV-CAG-FLEx^{loxP}-TC66T* and *AAV-CAG-FLEx^{loxP}-G* was injected into the VTA of 4-6-week-old mice. Two weeks later, RV*dG* was injected into the VTA, and virus allowed to spread for five days. For *in situ* hybridization, midbrain sections were stained with probes for *Gad1* and *Gad2*[6], and imaged on a Zeiss LSM780 microscope at 20× magnification. Imaging, histology and whole-brain quantification were performed as previously described[7]. In Fig. 5f, the VTA included the parabrachial pigmented area (PBP) and paranigral nucleus (PN). Data were averaged from three mice.

Coordinates used were (relative to Bregma, midline, or dorsal brain surface and in mm): VTA: AP −3.20, ML 0.4, DV −4.2; NAcLatS: AP +1.45, ML 1.75, DV −4.0; NAcMedS: AP +1.55, ML 0.7, DV −4.0; GPe: AP −0.35, ML 1.75, DV −3.5; SNr (midbrain): AP −3.2, ML 1.1, DV −4.5.

The titres of viruses, based on quantitative PCR analysis, were as follows: *AAV-CAG-FLEx^{loxP}-TC*, serotype 5, 2.4×10^{13} genome copies (gc)/ml; *AAV-CAG-FLEx^{loxP}-G*, serotype 8, 1.0×10^{12} gc/ml; *AAV-CAG-FLEx^{FRT}-TC*, serotype 5, 2.6×10^{12} gc/ml; *AAV-CAG-FLEx^{FRT}-G*, serotype 8, 1.3×10^{12} gc/ml; *AAV-CAG-FLEx^{loxP}-TC66T*, serotype 2, 1.0×10^{12} gc/ml; *AAV-hsyn1-FLEx^{loxP}-mGFP-2A-synaptophysin-mRuby*, serotype DJ, 9.3×10^{12} gc/ml; *AAV-hsyn1-FLEx^{loxP}-hM3Dq-mCherry*, serotype DJ, 4.0×10^{12}gc/ml; *AAV-hsyn1-FLEx^{loxP}-hM4Di-mCherry*, serotype DJ, 5.5×10^{12} gc/ml; *AAV-hsyn1-FLEx^{loxP}-K$_{ir}$2.1-T2A-GFP*, serotype DJ, 5.6×10^{13} gc/ml; *AAV-CMV-FLEx^{loxP}-eGFP-2A-TeTxLc*, serotype DJ, 2.1×10^{12} gc/ml; *AAV-hsyn1-FLEx^{loxP}-ChR2(H134R)-YFP*, serotype DJ, 1.4×10^{13} gc/ml; *AAV-hsyn1-FLEx^{loxP}-YFP*, serotype DJ, 1.5×10^{13} gc/ml; *AAV-EF1α-FLEx^{loxP}-GCaMP6f*, serotype 5, 1.9×10^{13} gc/ml; *AAV-hsyn1-FLEx^{FRT}-mGFP-2A-synaptophysin-mRuby*, serotype DJ, 3.7×10^{12} gc/ml; *AAV-hsyn1-FLEx^{FRT}-hM4Di-mCherry*, serotype DJ, 2.9×10^{13} gc/ml; *AAV-hsyn1-FLEx^{FRT}-hM3Dq-mCherry*, serotype DJ, 4.6×10^{13} gc/ml; *AAV-hsyn1-FLEx^{FRT}-K$_{ir}$2.1-T2A-GFP*, serotype DJ, 7.2×10^{13} gc/ml; *AAV-hsyn1-FLEx^{FRT}-ChR2(H134R)-YFP*, serotype DJ, 5.2×10^{12} gc/ml; *AAV-hsyn1-FLEx^{FRT}-YFP*, serotype DJ, 4.3×10^{12} gc/ml; *AAV-EF1α-FLEx^{FRT}-bReachES-mCherry*, serotype 5, 2.5×10^{13} gc/ml; *AAV-hsyn1-FLExOFF^{loxP}-hM4Di-mCherry*, serotype DJ, 1.1×10^{13} gc/ml; *AAV-hsyn1-FLExOFF^{loxP}-hM3Dq-mCherry*, serotype DJ, 1.2×10^{13} gc/ml; *AAV-hsyn1-FLExOFF^{loxP}-K$_{ir}$2.1-T2A-GFP*, serotype DJ, 7.8×10^{12} gc/ml; *AAV-hsyn1-FLExOFF^{loxP}-YFP*, serotype DJ, 1.4×10^{13} gc/ml; *CAV-FLEx^{loxP}-Flp*, 5.0×10^{12} gc/ml; RV*dG*, 5.0×10^{8} colony forming units (cfu)/ml (both GFP and mCherry).

Rabies input tracing and targeted input activity manipulations. To trace inputs from VTA-DA neurons while manipulating input regions, we used either *DAT-Cre;Pvalb-Flp* double heterozygotes (for GPe manipulations) or *DAT-Cre;A2a-Cre* double heterozygotes (for NAcMedS manipulations) between 4 and 6 weeks of age.

To manipulate GPe-PV neurons, in *DAT-Cre;Pvalb-Flp* mice, 100 nl of a 1:1 volume mixture of *AAV-CAG-FLEx^{loxP}-TC* and *AAV-CAG-FLEx^{loxP}-G* was injected into the VTA of both hemispheres, and 300 nl of *AAV-FLEx^{FRT}-hM4Di*, *AAV-FLEx^{FRT}-hM3Dq*, *AAV-FLEx^{FRT}-K$_{ir}$2.1*, or *AAV-FLEx^{FRT}-YFP* was injected into the GPe. Both hemispheres were used for each mouse, and counted independently. *AAV-FLEx^{FRT}-hM4Di* and *AAV-FLEx^{FRT}-hM3Dq* were injected into the same mice, as were *AAV-FLEx^{FRT}-K$_{ir}$2.1* and *AAV-FLEx^{FRT}-YFP*. One month later, RV*dG* was injected bilaterally into the VTA. To activate DREADDs, animals were injected once every 12 h with CNO for five days beginning immediately after RV*dG* injection.

To manipulate NAcMedS-D1 neurons, in *DAT-Cre;A2a-Cre* mice, 100 nl of a 1:1 volume mixture of *AAV-FLEx^{loxP}-TC* and *AAV-FLEx^{loxP}-G* was injected into the VTA of both hemispheres, and 300 nl of either *AAV-FLExOFF^{loxP}-hM4Di*, *AAV-FLExOFF^{loxP}-hM3Dq*, *AAV-FLExOFF^{loxP}-K$_{ir}$2.1*, or *AAV-FLExOFF^{loxP}-YFP* was injected into the NAcMedS. Both hemispheres were used for each mouse, and counted independently. *AAV-FLExOFF^{loxP}-hM4Di* and *AAV-FLExOFF^{loxP}-hM3Dq* were injected into the same mice, as were *AAV-FLExOFF^{loxP}-K$_{ir}$2.1* and *AAV-FLExOFF^{loxP}-YFP*. One month later, RV*dG* was injected bilaterally into the VTA.

For both GPe and NAcMedS manipulations, in mice injected with hM4Di-mCherry or hM3Dq-mCherry, an RV*dG* that expressed GFP was used; if the AAV expressed GFP or YFP, RV*dG* expressing mCherry was used.

Owing to the large sample sizes of the experiments involving targeted input activity manipulations, only inputs from the GPe and NAc were quantified. Inputs from the NAcCore and NAcLatS were used for normalization because the percentage of total rabies-labelled inputs from these regions was relatively invariant, regardless of whether injections were located more medially or laterally in the VTA[7], or whether a drug of abuse had been injected (Fig. 1, Extended Data Fig. 1a).

Rabies input tracing with two-day LMS procedure. To examine the relationship between rabies-labelled inputs in the GPe and locomotor sensitization to cocaine injections using a two-dose procedure, in *DAT-Cre* mice, 100 nl of a 1:1 volume mixture of *AAV-FLEx^{loxP}-TC* and *AAV-FLEx^{loxP}-G* was injected into the VTA. On days 1 and 2, mice received IP injections of saline and were habituated to an open field chamber equipped with infrared lasers for motion tracking. On day 3, mice were injected with one of the following: cocaine (15 mg/kg), amphetamine (1 mg/kg), nicotine (0.5 mg/kg) or morphine (10 mg/kg), and placed in the same open field chamber. On day 4, RV*dG* was injected into the VTA. On day 9, mice were injected with the same dose of the same drug they had received on day 3, and their locomotion was tracked in the open field. Experiments were terminated immediately thereafter. The rabies-labelled inputs into the GPe were quantified and normalized to the sum of inputs from the NAcLatS and NAcCore.

Axon projection quantification. Images were obtained and quantified as previously described[7], except that three sections were used for each region and were averaged to obtain the final value. Four brains were used for each experiment.

Synaptic puncta quantification. Methods for synaptic puncta quantification were adapted from Mosca and Luo[42] for use in mice. To quantify the volume and density of mRuby-labelled puncta from GPe-PV neuron termini in the SNr, 300 nl of *AAV-FLEx^{loxP}-mGFP-2A-synaptophysin-mRuby* was injected into the GPe of *Pvalb-Cre* mice, and sections were cut at a thickness of 60 μm. Floating sections were stained using anti-mCherry and anti-GFP antibodies. Sections were imaged on a Zeiss 510 confocal microscope using a 63× objective, with image stacks containing 30 sections at 0.44 μm intervals using 2× averaging and 2× optical zoom. Three images were taken of puncta in the SNr and subthalamic nucleus (STN) of each brain. Images were analysed using Imaris (Bitplane). The surface function was used to obtain the volume of mGFP$^+$ neurites and mRuby$^+$ puncta, while the spots function was used to estimate the number of mRuby$^+$ puncta. Data from the three slices from the SNr and STN were averaged for each brain. Measurements from the SNr were normalized to those from the STN.

Quantification of Fos immunostaining. To quantify integrated neural activity, Cre-dependent AAVs expressing YFP, hM4Di, ChR2 or K$_{ir}$2.1 were injected into the GPe of *Pvalb-Cre* mice and relative activation of VTA-DA neurons was measured by the ratio of Fos$^+$ neurons in the ventral midbrain that co-stained with TH to all Fos$^+$ neurons in the ventral midbrain (Fig. 5g–i). Animals were euthanized 90 min after the final stimulus (optical stimulation at 20 Hz for 30 min in ChR2-expressing animals, or cocaine or saline injection). When cocaine or saline was injected in animals expressing hM4Di, CNO was injected thirty minutes before the cocaine or saline injection. Animals were transcardially perfused, and

brains sectioned on a vibratome in PBS. Sections were blocked with 10% normal donkey serum (NDS) and 2% BSA/0.5% triton-X100 in PBS (PBST), then stained with TH and Fos antibodies in 1% NDS in PBST at 4 °C for four nights. Sections were rinsed three times for 30 min each at room temperature, followed by secondary antibody stain in 1% NDS in PBST at 4 °C for two nights. Sections were then rinsed three times for 30 min each, and mounted on slides. The midbrain from three representative VTA-containing sections were then imaged on a Zeiss LSM 780 confocal microscope at 20× magnification, and the results averaged together for each brain. For activation of GPe neurons for Fos immunostaining, 300 nl of *AAV-FLEx^{loxP}-ChR2* was injected bilaterally into the GPe of *Pvalb-Cre* mice, and 200 μm, 0.39NA optical fibres were implanted over the VTA. For stimulation, the optical fibre was connected to a 473 nm laser diode (OEM Laser systems) through an FC/PC adaptor. Laser output was controlled using a Master-8 pulse stimulation, which delivered 5 ms light pulses at 20 Hz. Light output through the optical fibres was adjusted to 20 mW using a digital power meter console. Images were taken with a constant exposure time. Cells with a visually identifiable nuclear label by eye were considered Fos$^+$.

Immunohistochemistry. The following primary antibodies were used: rat anti-mCherry, Life Sciences, 1:2,000; chicken anti-GFP, Aves Labs, 1:1,000; rabbit anti-TH, Millipore, 1:1,000; goat anti-Fos, Santa Cruz, 1:500. The following secondary antibodies were used from Jackson ImmunoResearch at a concentration of 1:250: donkey anti-chicken AlexaFluor488; donkey anti-goat AlexaFluor488; donkey anti-rat AlexaFluor555; donkey anti-goat AlexaFluor555; donkey anti-rabbit AlexaFluor647.

Fibre photometry. To assess cocaine-induced changes in neuronal activity *in vivo*, fibre photometry was used[43]. We injected 750 nl of *AAV-FLEx^{loxP}-GCaMP6f* into the GPe of *Pvalb-Cre* mice, and implanted a 400 μm diameter, 0.48NA optical fibre (Doric Lenses) at the same location. To test the effect of GPe-PV neuron stimulation on VTA-DA neuron activity, 300 nl of *AAV-FLEx^{FRT}-bReachES* was injected into the GPe, and 750 nl of *AAV-FLEx^{loxP}-GCaMP6f* was injected into the VTA of *DAT-Cre;Pvalb-Flp* mice. A 400 μm diameter, 0.48NA optical fibre was implanted over the VTA, and a 200 μm, 0.39NA fibre (made in-house) was implanted over the GPe. Implants were secured to the skull with metal screws (Antrin Miniature Specialists), Metabond (Parkell), and Geristore dental epoxy (DenMat). Mice were allowed to recover for at least 4 weeks before experiments.

Fibre photometry recordings were made using previously described equipment[9]. In brief, 405 nm and 470 nm excitation light was used to excite GCaMP6f at its isosbestic and calcium-dependent wavelengths to obtain both a control and calcium signal in the same animal, respectively. To activate bReachES-expressing GPe-PV neurons, a 594 nm laser was controlled by a Master-8 pulse stimulation (A.M.P.I.) that delivered 5 ms pulses at 40 Hz. Light output through the optical fibres was adjusted to 10 mW using a digital power meter console (Thorlabs). Light was manually switched on at 10 min and off at 20 min.

All data analysis was performed in MATLAB. Signals were first motion corrected by subtracting the least squares best fit of the control trace to the calcium signal. Data points containing large motion artefacts were then manually removed. To assess neural activity, the median absolute deviation (MAD) was calculated across the entire photometry trace during a given session. We conservatively defined a threshold of 6 × MAD to assess bouts of high neural activity. During each session, we calculated the percentage of time that the photometry trace was greater than or equal to 6 × MAD of the entire trace. For Fig. 2i–k $n = 11$, and Fig. 5k–m $n = 9$.

Whole-cell recordings. Mice were deeply anaesthetized with isoflurane, and coronal midbrain or GPe slices (250 μm) were prepared after intracardial perfusion with ice-cold artificial cerebrospinal fluid (ACSF) containing (in mM): 230 sucrose, 10 glucose, 25 $NaHCO_3$, 2.5 KCl, 1.2 NaH_2PO_4, 0.5 $CaCl_2$, 7 $MgCl_2$, and oxygenated with 95% O_2/5% CO_2. After 60 min of recovery, slices were transferred to a recording chamber and perfused continuously at 2–4 ml/min with oxygenated ACSF containing (in mM): 120 NaCl, 10 glucose, 25 $NaHCO_3$, 2.5 KCl, 1.2 NaH_2PO_4, 2.5 $CaCl_2$, 2.3 $MgCl_2$ at 30 °C. Patch pipettes (3.8–4.4 MΩ) were pulled from borosilicate glass (G150TF-4; Warner Instruments) and filled with internal solution containing (in mM): 131 $CsCH_3SO_3$, 10 HEPES, 10 glucose, 2 $CaCl_2$, 10 EGTA, 5 MgATP, 0.4 NaGTP, 10 phosphocreatine, 5 QX314, and 0.2% biocytin (pH 7.3, 292 mOsm) for voltage clamp recordings. For analysis of GPe excitability, the internal solution contained (in mM): 130 $KMeSO_3$, 9 KCl, 0.1 EGTA, 10 HEPES, 4 Mg-ATP, 0.4 Na-GTP, 7.5 Na_2-phosphocreatine, adjusted to pH 7.3 with KOH, 290–295 mOsm. Input resistance and access resistance were monitored continuously throughout each experiment; experiments were terminated if these changed by >20%.

Labelled neurons were visualized with a 40× water-immersion objective on an upright fluorescent microscope (BX51WI; Olympus) equipped with infrared-differential interference contrast video microscopy and epifluorescence (Olympus). ChR2 was stimulated by flashing 473-nm light (2 ms pulses, 0.1 Hz, 10 mW) through the light path of the microscope using an ultrahigh-powered light-emitting diode (LED) powered by an LED driver (Thorlabs) under computer control. The light intensity of the LED was not changed during the experiments. A dual lamp house adaptor (Olympus) was used to switch between the fluorescence lamp and LED light source.

For monosynaptic connectivity analysis, D-APV (50 μM) and NBQX (10 μM) were added to block NMDA receptors and AMPA receptors, respectively, and tetrodotoxin (TTX, 1 μM), a voltage-gated sodium channel antagonist, and 4-aminopyridine (4-AP, 1mM), a potassium channel antagonist, were added to isolate monosynaptic connections[44]. The IPSC amplitude plotted in Fig. 5c included only cells with detectable optically evoked IPSCs.

For analysis of quantal size and frequency from GPe inputs to SNr neurons, we replaced calcium in the ACSF with 4 mM $SrCl_2$ to induce asynchronous vesicle release. The amplitude and frequency of events occurring between 50 ms and 250 ms after the blue light pulse were recorded. The amplitude of each event was measured from a local baseline established 5–10 ms before the light pulse. All electrophysiology data were collected using Axograph software.

Behavioural assays of LMS and CPP. To test the necessity of GPe-PV neuron activity for the development of LMS or CPP, 300 nl of *AAV-FLEx^{loxP}-hM4Di*, *AAV-FLEx^{loxP}-K$_{ir}$2.1*, *AAV- FLEx^{loxP}-TeTxLc*, or *AAV-FLEx^{loxP}-YFP* was injected bilaterally into the GPe of *Pvalb-Cre* animals.

To assay for drug-induced CPP, animals were first tested in a single drug pairing, two-chamber CPP test. Each chamber was given either a clear, textured or black, smooth floor. On the first day, animals were initially placed into the right chamber, and allowed to freely explore both chambers for thirty minutes (pre-test). On the second day, animals were saline-conditioned to the left side, and on the following day, cocaine (or morphine)-conditioned to the right side. Drug conditioning on the black, smooth or clear, textured floor was counterbalanced across the mice. On the fourth day, animals were again initially placed into the right chamber, and allowed to explore freely (post-test). For animals injected with CNO, 10 mg/kg CNO was injected thirty minutes before the beginning of the cocaine and saline pairings.

The following week, to test LMS, animals were habituated to open field boxes equipped with motion tracking for two days (receiving saline injections before each session). Animals were then injected with cocaine (or morphine) immediately before entry into the open-field boxes, for five consecutive days, for 30 min each. For animals injected with CNO, CNO was delivered 30 min before the beginning of each session. In Extended Data Fig. 5, both YFP and hM4Di-expressing animals were given CNO 30 min before morphine injection.

To inhibit GPe-PV neurons that project to the midbrain, 500 nl of *CAV2-FLEx^{loxP}-Flp* was injected into the SNr, and 300 nl of *AAV-FLEx^{FRT}-K$_{ir}$2.1* was injected into the GPe of *Pvalb-Cre* mice. All injections were bilateral. Animals were tested 2 weeks later.

To inhibit GPe-PV terminals in the midbrain, animals were injected with 300 nl of *AAV-FLEx^{loxP}-YFP* or *AAV-FLEx^{loxP}-hM4Di* in the GPe, and a bilateral cannula guide (C235G, 26GA, C/C distance 1.8 mm, 5 mm pedestal, cut 3.5 mm below pedestal, custom specified for mouse bilateral ventral midbrain coordinates, Plastics One) was implanted over the ventral midbrain (coordinates AP −3.5, ML 0.9, DV −3.13). Two skull screws were implanted for headcap stability, and headcaps were sealed with Metabond and Geristore. CNO microspheres were synthesized to enable slow release of CNO after a single infusion. Degradex PLGA CNO microspheres were custom ordered from Phosphorex. Beads of target mean diameter 1 μm were dissolved in 0.5% trehalose at a concentration of 5 mg microsphere per ml. The estimated CNO loading efficiency was 5%, the estimated burst release was 50%, and the estimated release time was 7 days. The target concentration of CNO release at a steady state was 100 pg/h[23,45].

On day 1 of the behavioural protocols, animals were given an IP saline injection. On day 2, one hour before locomotor testing, all cannula guides were pierced with a dummy infuser (C235I, 33GA, project 1.5 MM past guide), and mice were given an IP saline injection one hour later. On day 3, CNO microspheres were infused one hour before locomotor testing, 250 nl per side at 250 nl/min, and mice were given an IP saline injection one hour later and tested for effects on basal locomotion. On days 3–6, animals were run through the CPP protocol, and on days 6–10 (starting on the same afternoon) they were run through the LMS protocol. We then waited a week for CNO washout, and repeated the standard CPP and LMS procedures without subsequent infusions in hM4Di-expressing animals.

For manipulations of SNr-GABA neurons, 500 nl of *AAV-FLEx^{loxP}-hM3Dq* was injected bilaterally into the SNr of *GAD2-Cre* mice, or 500 nl of *AAV-FLEx^{loxP}-hM4Di* was injected into the SNr and 300 nl of *AAV-FLEx^{FRT}-K$_{ir}$2.1* was injected into the GPe of *GAD2-Cre;Pvalb-Flp* animals. All injections were bilateral.

Data analyses and statistics. All statistics were calculated using GraphPad Prism 7 software. Statistical significance was assessed by paired *t*-tests with the exception of Fig. 2n, where a two-way ANOVA was used, and Figs 2k and 5m where a one-way ANOVA was used with the Geisser–Greenhouse correction followed by *post hoc*

Wilcoxon matched-pairs signed rank tests. Dot plots presented throughout the manuscript include a horizontal line representing the mean value for each group. In Fig. 1 and Extended Data Fig. 1, the length of each bar represents the mean. Error bars represent s.e.m. throughout. For all figures, NS $P > 0.05$, $*P \leq 0.05$, $**P \leq 0.01$, $***P \leq 0.001$, $****P \leq 0.0001$.

Data availability. Numerical data for each figure are included with the manuscript as source data. All other data are available from the authors upon reasonable request.

34. Bäckman, C. M. *et al.* Characterization of a mouse strain expressing Cre recombinase from the 3′ untranslated region of the dopamine transporter locus. *Genesis* **44,** 383–390 (2006).
35. Taniguchi, H. *et al.* A resource of Cre driver lines for genetic targeting of GABAergic neurons in cerebral cortex. *Neuron* **71,** 995–1013 (2011).
36. Hippenmeyer, S. *et al.* A developmental switch in the response of DRG neurons to ETS transcription factor signaling. *PLoS Biol.* **3,** e159 (2005).
37. Madisen, L. *et al.* Transgenic mice for intersectional targeting of neural sensors and effectors with high specificity and performance. *Neuron* **85,** 942–958 (2015).
38. Rothwell, P. E. *et al.* Autism-associated neuroligin-3 mutations commonly impair striatal circuits to boost repetitive behaviors. *Cell* **158,** 198–212 (2014).
39. Shuen, J. A., Chen, M., Gloss, B. & Calakos, N. Drd1a-tdTomato BAC transgenic mice for simultaneous visualization of medium spiny neurons in the direct and indirect pathways of the basal ganglia. *J. Neurosci.* **28,** 2681–2685 (2008).
40. Krashes, M. J. *et al.* Rapid, reversible activation of AgRP neurons drives feeding behavior in mice. *J. Clin. Invest.* **121,** 1424–1428 (2011).
41. Xue, M., Atallah, B. V. & Scanziani, M. Equalizing excitation-inhibition ratios across visual cortical neurons. *Nature* **511,** 596–600 (2014).
42. Mosca, T. J. & Luo, L. Synaptic organization of the *Drosophila* antennal lobe and its regulation by the Teneurins. *eLife* **3,** e03726 (2014).
43. Gunaydin, L. A. *et al.* Natural neural projection dynamics underlying social behavior. *Cell* **157,** 1535–1551 (2014).
44. Petreanu, L., Mao, T., Sternson, S. M. & Svoboda, K. The subcellular organization of neocortical excitatory connections. *Nature* **457,** 1142–1145 (2009).
45. Park, J. S. *et al.* Synthetic control of mammalian-cell motility by engineering chemotaxis to an orthogonal bioinert chemical signal. *Proc. Natl Acad. Sci. USA* **111,** 5896–5901 (2014).

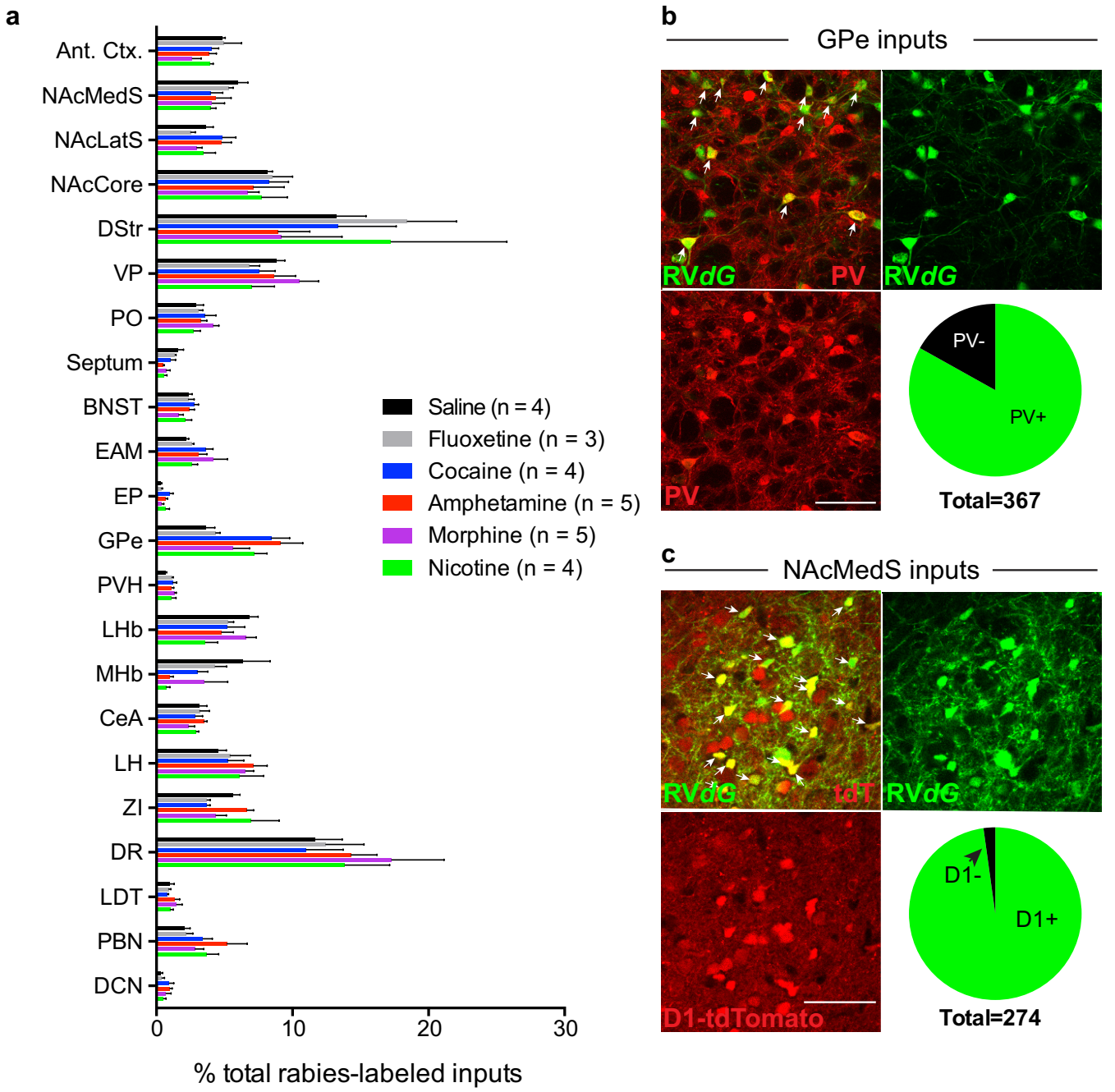

Extended Data Figure 1 | Changes to VTA-DA inputs induced by drugs of abuse. a, Quantification of monosynaptic inputs to VTA-DA neurons labelled in animals receiving single dose administration of cocaine, amphetamine, nicotine, morphine, saline, or fluoxetine one day before injection of RV*dG* into the VTA. Data were combined to generate Fig. 1c. **b**, Sample images of GPe neurons labelled by RV*dG* and co-stained for parvalbumin. Pie graph shows proportion of labelled cells that co-stained for parvalbumin. **c**, Sample images of NAcMedS neurons labelled by RV*dG* in *DAT-Cre;D1-tdTomato* mice. Pie graph shows proportion of labelled cells that were $D1^+$ as defined by presence of tdTomato (scale bars, 50 μm).

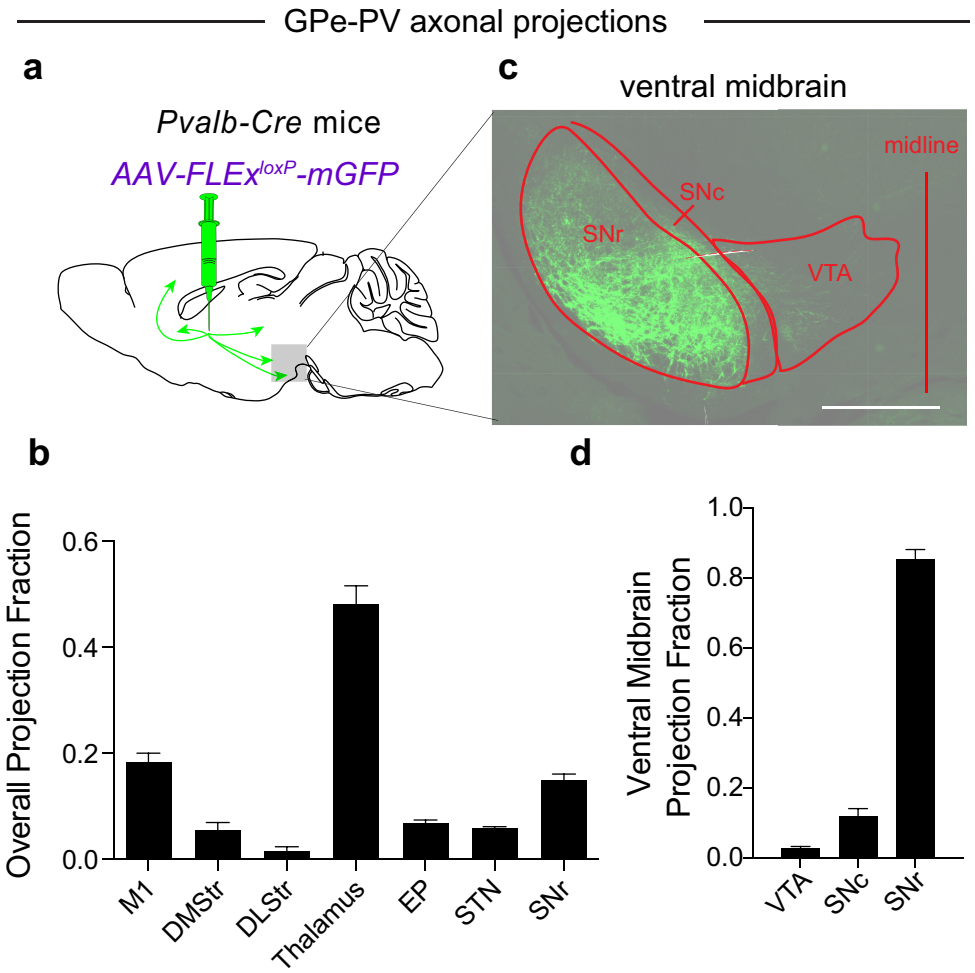

Extended Data Figure 2 | Axonal projections of GPe-PV neurons. **a**, *AAV-FLEx^{loxP}-mGFP* was injected into the GPe of *Pvalb-Cre* animals, and mGFP^{+} axons were quantified throughout the brain. **b**, Quantification of fraction of mGFP^{+} axons in the indicated brain regions. **c**, Sample image of mGFP^{+} axons in the ventral midbrain (scale bar, 500 μm). **d**, Quantification of fraction of mGFP^{+} axons in the indicated ventral midbrain brain regions. The schematics of the mouse brain in this figure were adapted from ref. 33. DLStr, dorsolateral striatum; DMStr, dorsomedial striatum.

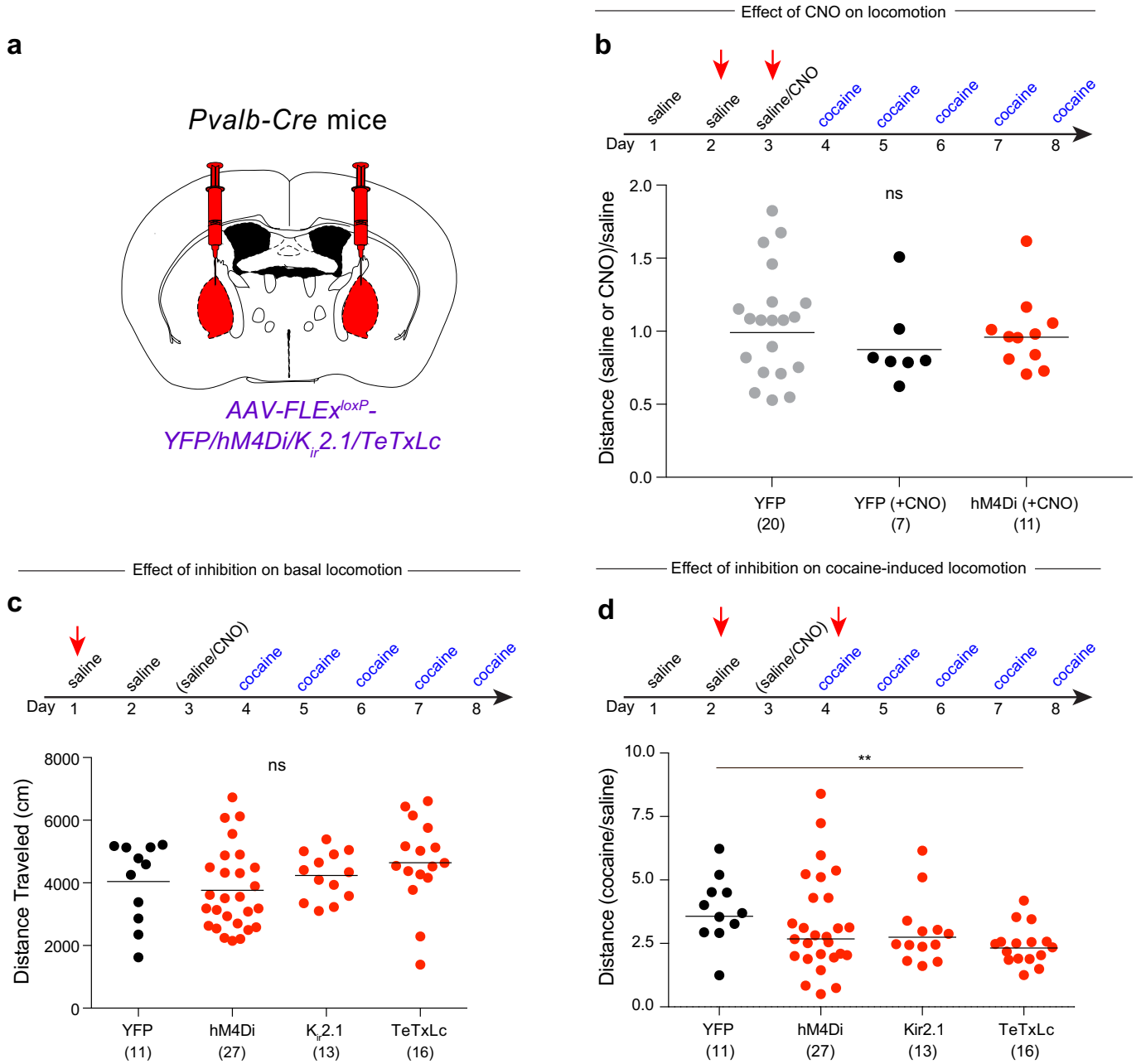

Extended Data Figure 3 | Inhibition of GPe-PV neuron activity modestly affects cocaine-induced locomotion. a, Cre-dependent AAVs expressing YFP, hM4Di, $K_{ir}2.1$ or TeTxLc were injected into the GPe of *Pvalb-Cre* animals. **b**, Quantification of effects of CNO on basal locomotion in animals expressing YFP or hM4Di (compared to YFP + saline: YFP + CNO, $P = 0.36$; hM4Di + CNO, $P = 0.59$). **c**, Quantification of basal locomotion during GPe-PV neuron inhibition (hM4Di, $P = 0.54$; $K_{ir}2.1$, $P = 0.66$; TeTxLc, $P = 0.27$). **d**, Quantification of cocaine-induced locomotion during GPe-PV neuron inhibition (hM4Di, $P = 0.37$; $K_{ir}2.1$, $P = 0.12$; TeTxLc, $P = 0.002$). The schematics of the mouse brain in this figure were adapted from ref. 33.

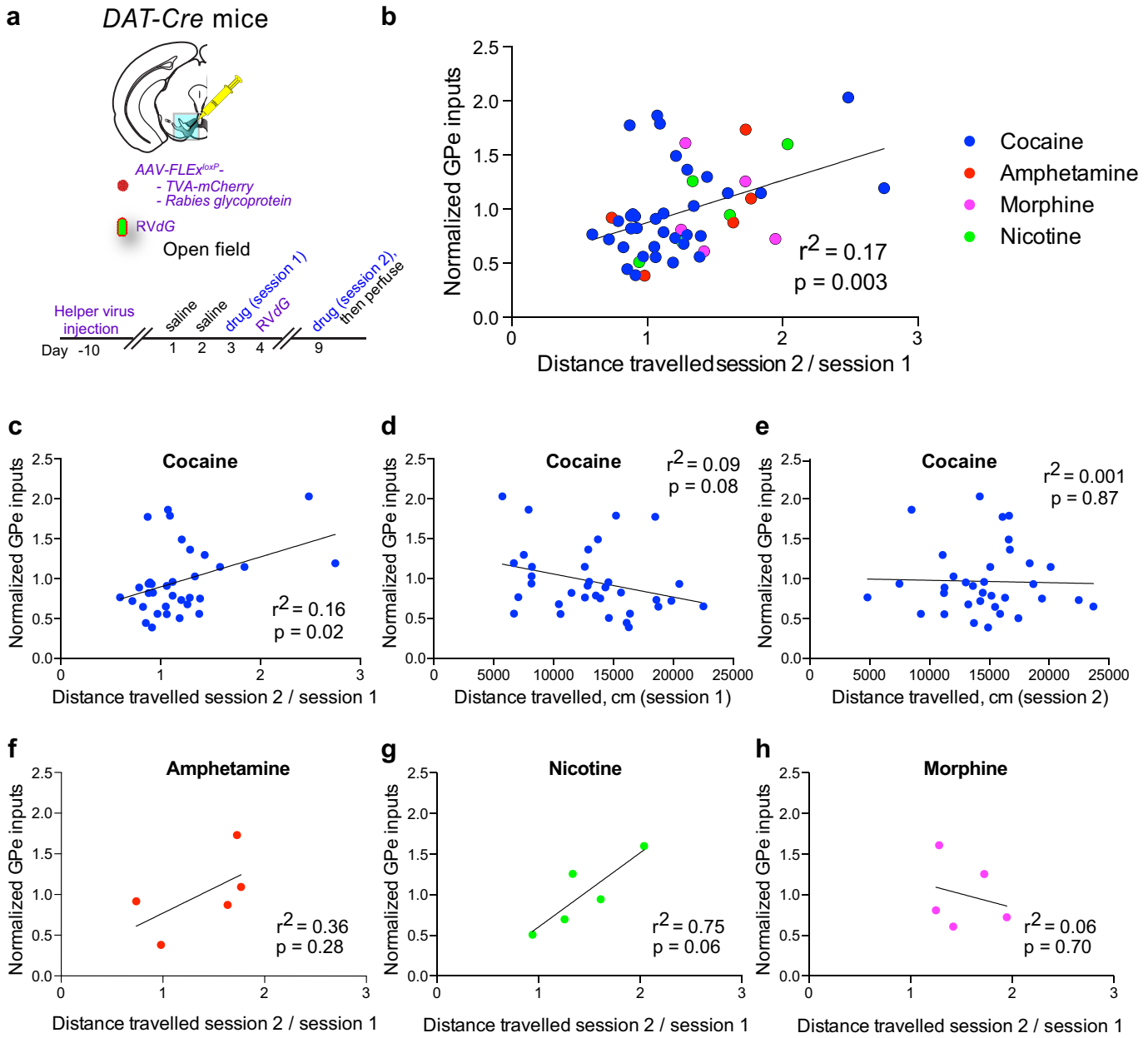

Extended Data Figure 4 | Labelled GPe inputs to the VTA correlated with LMS. a, *AAV-FLEx^{loxP}-TC* and *AAV-FLEx^{loxP}-G* were injected into the VTA of *DAT-Cre* mice. Eleven days later, animals were habituated for two days to an open field chamber, and given a drug injection the following day. RV*dG* was injected one day after the drug. Five days after RV*dG* injection, the animal was given a second injection of the same drug in the open field. **b**, Normalized labelled GPe inputs plotted against the relative locomotion in session 2 vs. session 1 for cocaine ($n = 34$), amphetamine ($n = 5$), nicotine ($n = 5$) and morphine ($n = 5$). Regression line is plotted for all drugs combined. **c**–**e**, Labelled GPe inputs after a single dose of cocaine significantly correlated with LMS (**c**) but not total locomotion after the first (**d**) or second (**e**) dose of cocaine. **f**–**h**, Plots of labelled GPe inputs vs. LMS for amphetamine (**f**; 1 mg kg^{-1}), nicotine (**g**; 0.5 mg kg^{-1}), or morphine (**h**; 10 mg kg^{-1}). The schematics of the mouse brain in this figure were adapted from ref. 33.

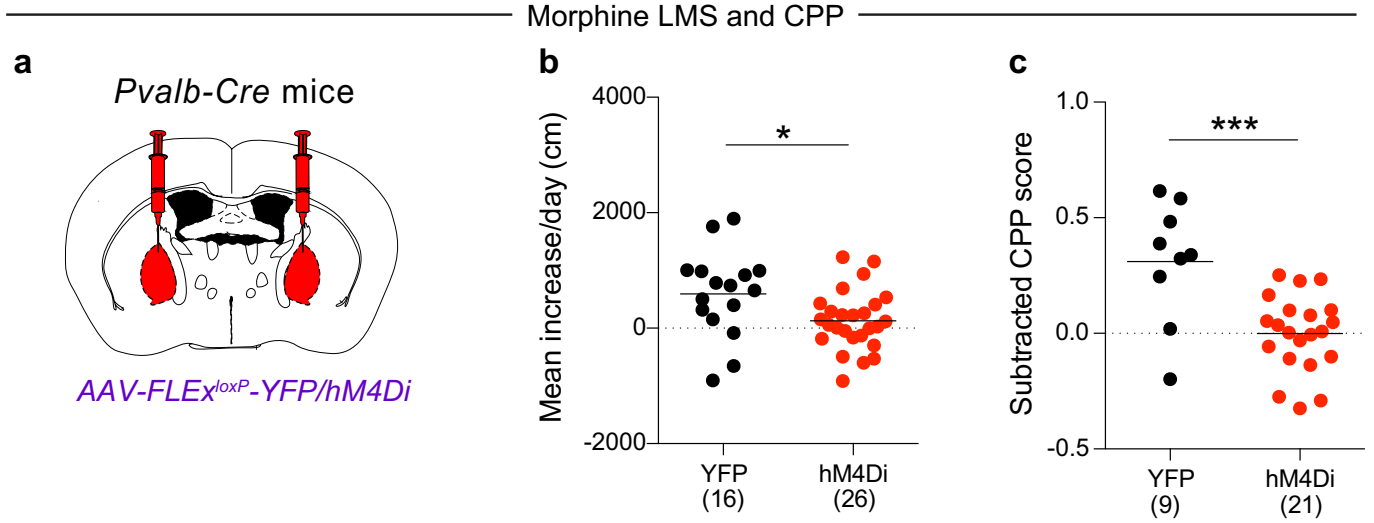

Extended Data Figure 5 | Inhibition of the GPe prevents morphine LMS and CPP. a, A Cre-dependent AAV expressing either YFP or hM4Di was injected into the GPe of *Pvalb-Cre* mice. **b**, **c**, Quantification of LMS (**b**; $P = 0.022$) and CPP (**c**; $P = 0.0005$) in animals in which YFP or hM4Di (activated by CNO) were expressed in GPe-PV neurons. The schematics of the mouse brain in this figure were adapted from ref. 33.

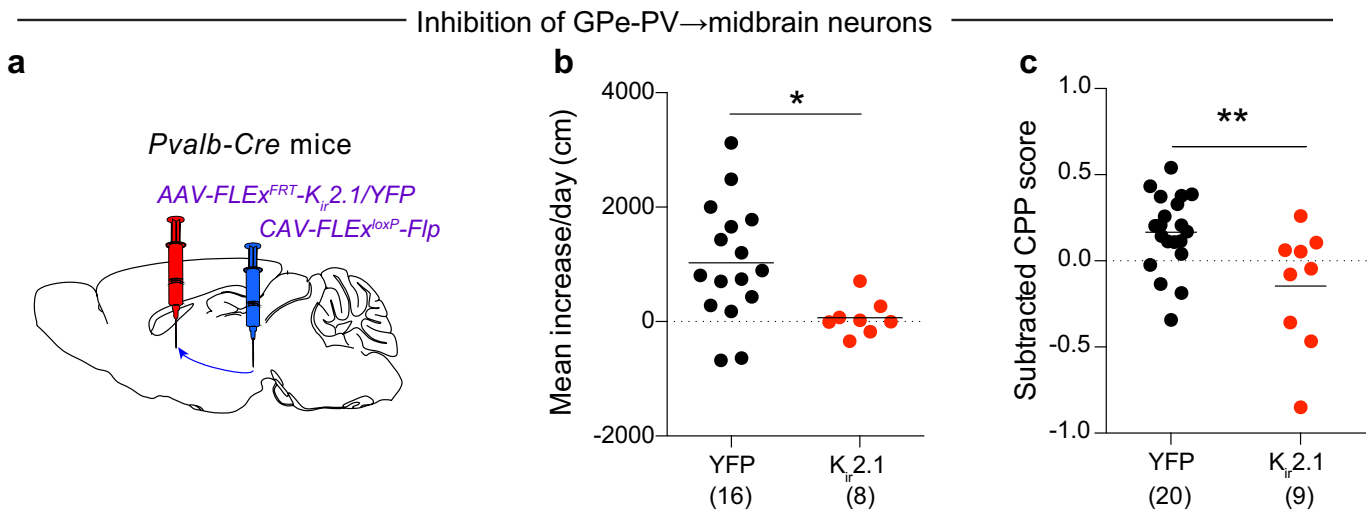

Extended Data Figure 6 | Inhibition of GPe-PV neurons that project to the midbrain blocks cocaine-induced CPP and LMS. a, *CAV-FLEx^{loxP}-Flp* was injected into the ventral midbrain, and *AAV-FLEx^{FRT}-K$_{ir}$2.1* or *AAV-FLEx^{FRT}-YFP* was injected into the GPe of *Pvalb-Cre* mice. **b**, **c**, Quantification of LMS (**b**; $P = 0.019$) and CPP (**c**; $P = 0.0067$) in animals in which YFP or $K_{ir}2.1$ were expressed in GPe-PV neurons projecting to the ventral midbrain. The schematics of the mouse brain in this figure were adapted from ref. 33.

GPe-PV→midbrain collaterals

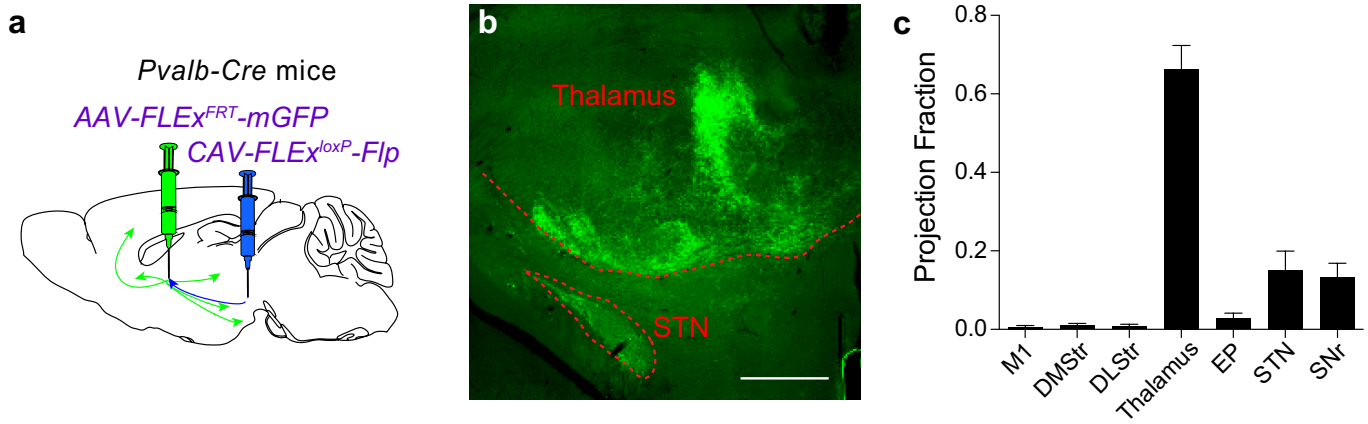

Extended Data Figure 7 | GPe-PV neurons that project to the midbrain collateralize to multiple subcortical targets. a, *CAV-FLEx^{loxP}-Flp* was injected into the ventral midbrain, and *AAV-FLEx^{FRT}-mGFP* was injected into in the GPe of *Pvalb-Cre* mice. **b**, Representative image of mGFP^{+} collaterals in the thalamus and subthalamic nucleus (STN) (scale bar, 500 μm). **c**, Quantification of projection fraction of collaterals to indicated target regions. The schematics of the mouse brain in this figure were adapted from ref. 33.

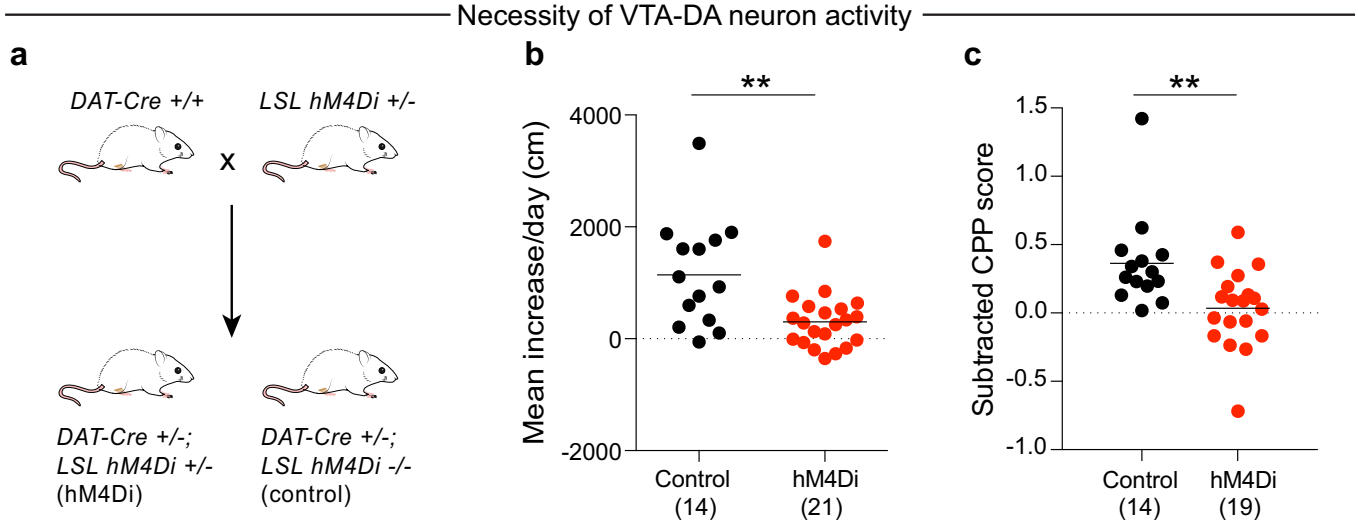

Extended Data Figure 8 | Dopamine neuron activity is required for the development of LMS and CPP. a, Breeding scheme for experiments. *LSL*, *loxP stop loxP*. **b**, **c**, Quantification of LMS (**b**; $P = 0.001$) and CPP (**c**; $P = 0.005$) in control animals or animals expressing hM4Di in dopamine neurons receiving CNO.

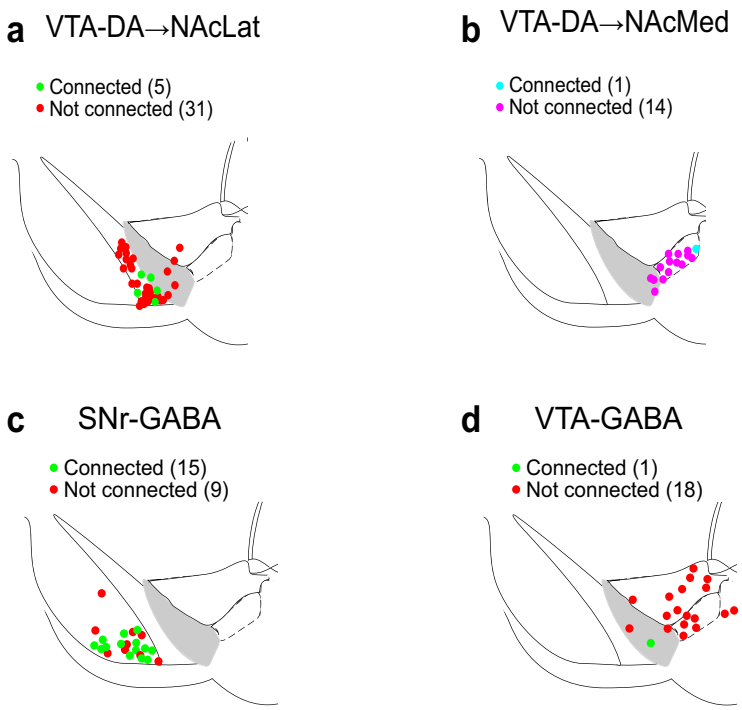

Extended Data Figure 9 | Map of anatomical location of ventral midbrain cells from which whole cell recordings were made. Individual dots indicate location of cells in which ChR2-evoked IPSCs due to ChR2 expression in GPe-PV neurons could be detected (connected) or not (not connected) in NAcLat-projecting (**a**) or NAcMed-projecting (**b**) VTA-DA cells, and SNr-GABA (**c**) or VTA-GABA (**d**) cells. The schematics of the mouse brain in this figure were adapted from ref. 33.

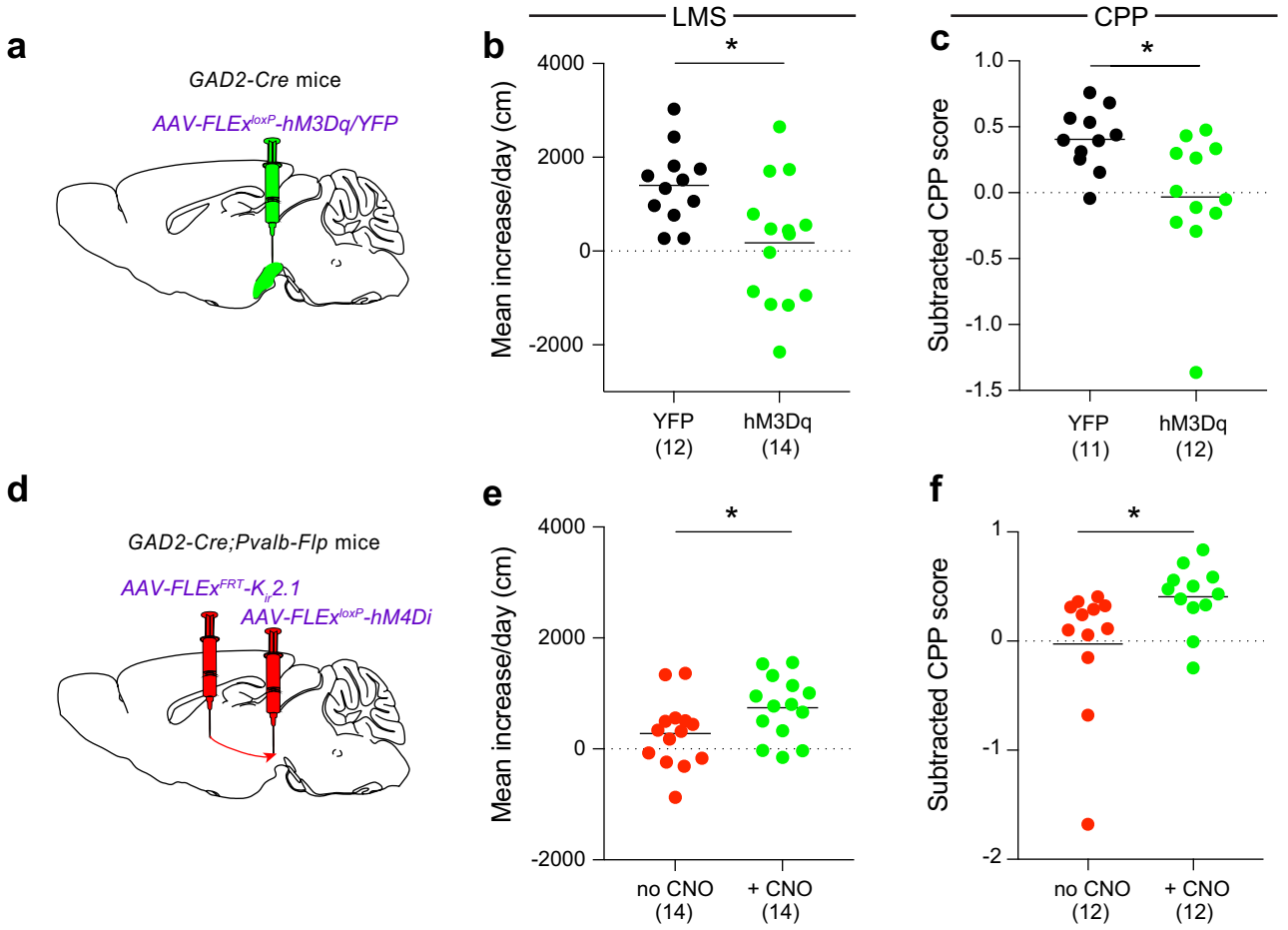

Extended Data Figure 10 | GPe-PV neurons mediate their effects through SNr-GABA neurons. a, Procedure to test LMS and CPP during SNr-GABA activation. **b**, **c**, Activating SNr-GABA neurons with CNO prevented LMS (**b**; $P = 0.010$) and CPP (**c**; $P = 0.015$). **d**, Injection strategy to test whether SNr-GABA neurons are downstream of GPe-PV neurons. **e**, **f**, While expression of $K_{ir}2.1$ in GPe-PV neurons prevented LMS and CPP, this suppression was overcome by concurrent inhibition of SNr-GABA neurons (**e**; $P = 0.035$, **f**; $P = 0.036$). The schematics of the mouse brain in this figure were adapted from ref. 33.

nature research

Corresponding author(s): Robert C. Malenka, Liqun Luo

☐ Initial submission ☒ Revised version ☐ Final submission

Life Sciences Reporting Summary

Nature Research wishes to improve the reproducibility of the work that we publish. This form is intended for publication with all accepted life science papers and provides structure for consistency and transparency in reporting. Every life science submission will use this form; some list items might not apply to an individual manuscript, but all fields must be completed for clarity.

For further information on the points included in this form, see Reporting Life Sciences Research. For further information on Nature Research policies, including our data availability policy, see Authors & Referees and the Editorial Policy Checklist.

Experimental design

1. Sample size

Describe how sample size was determined.	No statistical methods were used to predetermine sample size.

2. Data exclusions

Describe any data exclusions.	Data were excluded only in experiments where viral injections were performed and post-hoc analysis of viral targeting demonstrated that injections were inaccurate.

3. Replication

Describe whether the experimental findings were reliably reproduced.	Results described throughout the paper were reproduced. Multiple rounds of experimentation were required, and multiple methods were used where applicable (e.g., multiple drugs of abuse show similar increases in rabies-labeled GPe inputs, Extended Data Fig. 1, and multiple methods of GPe inhibition all block LMS and CPP, Fig. 4). No issues were identified in replicating any of the reported findings.

4. Randomization

Describe how samples/organisms/participants were allocated into experimental groups.	Experiments described in Fig.'s 1, 2a-h and 2l-n, 3, 5g-j and Extended Data Figs. 1a, 4, 5, 6, 8, and 10 were randomized and investigators were blinded to allocation and outcome assessments; all other experiments were not randomized and investigators were not blinded.

5. Blinding

Describe whether the investigators were blinded to group allocation during data collection and/or analysis.	Experiments described in Fig.'s 1, 2a-h and 2l-n, 3, 5g-j and Extended Data Figs. 1a, 4, 5, 6, 8, and 10 were randomized and investigators were blinded to allocation and outcome assessments; all other experiments were not randomized and investigators were not blinded.

Note: all studies involving animals and/or human research participants must disclose whether blinding and randomization were used.

6. Statistical parameters

For all figures and tables that use statistical methods, confirm that the following items are present in relevant figure legends (or in the Methods section if additional space is needed).

n/a	Confirmed
☐	☒ The exact sample size (*n*) for each experimental group/condition, given as a discrete number and unit of measurement (animals, litters, cultures, etc.)
☐	☒ A description of how samples were collected, noting whether measurements were taken from distinct samples or whether the same sample was measured repeatedly
☒	☐ A statement indicating how many times each experiment was replicated
☐	☒ The statistical test(s) used and whether they are one- or two-sided (note: only common tests should be described solely by name; more complex techniques should be described in the Methods section)
☐	☒ A description of any assumptions or corrections, such as an adjustment for multiple comparisons
☐	☒ The test results (e.g. *P* values) given as exact values whenever possible and with confidence intervals noted
☐	☒ A clear description of statistics including central tendency (e.g. median, mean) and variation (e.g. standard deviation, interquartile range)
☐	☒ Clearly defined error bars

See the web collection on statistics for biologists for further resources and guidance.

Software

Policy information about availability of computer code

7. Software

Describe the software used to analyze the data in this study.	MATLAB software was used to analyze fiber photometry data All electrophysiology data were collected using Axograph software. GraphPad Prism was used to analyze all other data.

For manuscripts utilizing custom algorithms or software that are central to the paper but not yet described in the published literature, software must be made available to editors and reviewers upon request. We strongly encourage code deposition in a community repository (e.g. GitHub). *Nature Methods* guidance for providing algorithms and software for publication provides further information on this topic.

Materials and reagents

Policy information about availability of materials

8. Materials availability

Indicate whether there are restrictions on availability of unique materials or if these materials are only available for distribution by a for-profit company.	There are no restrictions on materials.

9. Antibodies

Describe the antibodies used and how they were validated for use in the system under study (i.e. assay and species).	The following primary antibodies were used: Rat anti-mCherry, Life Sciences, 1:2000; chicken anti-GFP, Aves Labs, 1:1000; rabbit anti-TH, Millipore, 1:1000; Goat anti-Fos, Santa Cruz, 1:500. The following secondary antibodies were used from Jackson ImmunoResearch at a concentration of 1:250: donkey anti-chicken AlexaFluor488; donkey anti-goat AlexaFluor488; donkey anti-rat AlexaFluor555; donkey anti-goat AlexaFluor555; donkey anti-rabbit AlexaFluor647. Antibodies were validated 1. In the case of an extensively published antibody, by testing the specificity of staining to the appropriate regions (e.g. tyrosine hydroxylase, TH), or 2. by comparing between animals (e.g. cFos) and noting labeling that is above background but not consistent with non-specific staining.

10. Eukaryotic cell lines

a. State the source of each eukaryotic cell line used. N/A

b. Describe the method of cell line authentication used. N/A

c. Report whether the cell lines were tested for mycoplasma contamination. N/A

d. If any of the cell lines used are listed in the database of commonly misidentified cell lines maintained by ICLAC, provide a scientific rationale for their use. N/A

Animals and human research participants

Policy information about studies involving animals; when reporting animal research, follow the ARRIVE guidelines

11. Description of research animals

Provide details on animals and/or animal-derived materials used in the study.

Mice were housed on a 12-hour light/dark cycle with food and water ad libitum. Males and females from a mixed CD1 and C57/BL6 background were used for all experiments in approximately equal proportions. All surgeries were done under isoflurane anesthesia. All procedures complied with the animal care standards set forth by the National Institute of Health and were approved by Stanford University's Administrative Panel on Laboratory Animal Care and Administrative Panel of Biosafety.

Policy information about studies involving human research participants

12. Description of human research participants

Describe the covariate-relevant population characteristics of the human research participants.

N/A